Hydrodynamics and mass transfer characteristics of gas–liquid ejectors

S. Balamurugan, Mayank D. Lad, Vilas G. Gaikar, Ashwin W. Patwardhan *

Chemical Engineering Department, Institute of Chemical Technology, University of Mumbai, Matunga, Mumbai 400019, India

Abstract

In the present work, experimental investigations have been carried out on ejectors employing air as a motive fluid and water as the entrained fluid. A semi-empirical model has been developed to predict the liquid entrainment rate taking into account: (i) the compressible nature of air, (ii) pressure drop for two-phase flow and (iii) losses due to changes in cross sectional area. The effects of gas velocity, liquid level in the suction chamber, nozzle diameter and throat diameter on the liquid entrainment, entrainment ratio (L/G), pressure drop, gas hold-up, mass transfer coefficient and interfacial area have been investigated. The liquid entrainment rate increases with the increased liquid level in the suction chamber and with the increase in gas velocity. The ratio of throat cross sectional area to the nozzle cross sectional area (area ratio) was found to be a critical parameter. These results have been explained on the basis of pressure profiles of ejector (along the centre line of the ejector). The liquid entrainment rate predicted from the semi-empirical model is in good agreement with the experimental values. The mass transfer coefficient and interfacial area increase with increase in gas velocity. Correlations have been proposed to estimate the fractional gas hold-up, mass transfer coefficient and interfacial area in the ejectors.
© 2007 Elsevier B.V. All rights reserved.

Keywords: Hydrodynamics; Multiphase flow; Ejector; Mass transfer; Entrainment; Pressure drop

1. Introduction

Ejectors are co-current flow systems, where simultaneous aspiration and dispersion of the entrained fluid takes place. This causes continuous formation of fresh interface and generation of large interfacial area because of the entrained fluid between the phases. The ejector essentially consists of an assembly comprising of nozzle, converging section, mixing tube/throat and diffuser. According to the Bernoulli's principle, when a motive fluid is pumped through the nozzle of a gas–liquid ejector at a high velocity, a low pressure region is created just outside the nozzle. A second fluid gets entrained into the ejector through this low pressure region. The dispersion of the entrained fluid in the throat of the ejector with the motive fluid jet emerging from the nozzle leads to intimate mixing of the two phases. A diffuser section after the mixing tube/throat helps in the pressure recovery. The motive fluid jet performs two functions; one, it develops the suction for the entrainment of the secondary fluid and the second, it provides energy for the dispersion of one phase into the

other. This process has largely been exploited in vacuum systems in which a high speed fluid stream (typically steam) is used to generate vacuum. Ejectors also produce higher mass transfer rates by generating very small bubbles/droplets of the dispersed phase, thereby improving the contact between phases, which can then be injected into a reaction vessel [1]. Compared to the other gas–liquid contacting systems like stirred tanks and bubble columns, ejectors provide higher values of volumetric mass transfer coefficient [2,3]. In chemical industries, ejectors are also used to entrain and pump corrosive liquids, slurries, fumes and dust-laden gases, which otherwise are difficult to handle [4]. Jet ejectors can also be used for mass transfer operations like gas absorption or stripping [5].

High values of mass transfer coefficient and interfacial area enable a substantial reduction in the size (and hence capital cost) of a mass transfer contactor. The benefits are particularly important if the intrinsic rates of chemical reactions accompanying the mass transfer operations are very high and a mass transfer controlled regime prevails. For example, in the chemical exchange process producing heavy water [6], a synthesis gas mixture of nitrogen and hydrogen is contacted with liquid ammonia at high pressure and low temperature conditions. The deuterium absorption from the gas mixture into the liquid

* Corresponding author. Tel.: +91 22 2414 5616; fax: +91 22 2414 5614.
  E-mail address: awp@udct.org (A.W. Patwardhan).

Nomenclature

a	gas–liquid interfacial area (m^2/m^3)
A, a	cross sectional area as denoted in the subscript (m^2)
A_r	area ratio $(D_T/D_N)^2$
A_r'	area ratio of nozzle inlet to nozzle tip
C_0	constant used to estimate gas hold-up in bubble column
C_1	slip velocity in bubble column (m/s)
$[CO_2^*]$	solubility of CO_2 at gas–liquid inter-phase (kmol/m^3)
$[CO_2]_0$	solubility of CO_2 in bulk-phase (kmol/m^3)
D_{CO_2}	diffusivity of CO_2 in the solution (m^2/s)
D_B	diameter of bubble (m)
D_C	diameter of column (m)
D_D	diameter of diffuser (m)
D_{EC}	diameter of converging section after the nozzle exit (m)
D_I	impeller diameter (m)
D_N	diameter of nozzle tip (m)
D_{NaOH}	diffusivity of NaOH (m^2/s)
D_P	diameter of droplet (m)
D_s	diameter of stirred tank (m)
D_T	diameter of throat (m)
D_0	nozzle inlet diameter (m)
e_D	rate of energy dissipation (W/kg)
f_e	fraction of total suction utilized for entrained fluid dispersion
f_L	friction factor from liquid velocity
f_1, f_2	friction factor for single-phase flow
Fl	flow number
Fr	Froude number
F_1, F_2, F_3	fluid forces on solid wall (N)
g	acceleration due to gravity (m/s^2)
G	gas volumetric flow rate (m^3/s)
G^*	air mass flux at choked condition (kg/m^{2}s)
h	liquid height from nozzle tip to liquid surface (m)
H	Henrys' constant (kmol/m^{3}atm)
H_c	height of ejector (m)
H_D	height of diffuser (m)
H_{ST}	straight tube height from diffuser outlet (m)
H_T	throat height (m)
I_G	gamma ray intensity in empty column
I_L	gamma ray intensity in column filled with liquid only
I_{TP}	gamma ray intensity in two-phase
k	proportionality constant
k_L	true mass transfer co-efficient (m/s)
k_La	liquid side mass transfer co-efficient (1/s)
k_2	rate of reaction
K_C	loss coefficient in converging section
K_D	expansion loss coefficient in diffuser section
K_{ejt}	loss coefficient of total ejector [14]
K_I	loss coefficient ($K_I = 1 + K_T - \eta_{DU}$)
K_N	loss coefficient of nozzle
K_S	loss coefficient of throat entrance (for entrained fluid)
K_T	loss coefficient of the throat
K_2	fitted constant
K', K'', K_1'	loss coefficient
l	liquid hold-up
L	liquid volumetric flow rate (m^3/s)
LH	liquid level (m)
M_r	mass ratio (mass flow rate of entrained fluid/mass flow rate of motive fluid)
M	molecular weight (kg/kmol)
$\sqrt{M}$	rate of the amount of CO_2 reacting in the film to that reacting in the bulk buffer solution
n	power law constant
$[Na_2Co_3]_0$	sodium carbonate concentration (kmol/m^3)
$[O_2^*]$	solubility of O_2 (kmol/m^3)
$[O_2]_0$	initial concentration of O_2 (kmol/m^3)
P, p	pressure (N/m^2)
P_{IN}	supply pressure (N/m^2)
P_N	pressure at the nozzle tip (N/m^2)
PP	partial pressure (N/m^2)
P/V	power input per unit volume (kW/m^3)
(ΔP)	pressure drop (N/m^2)
$(\Delta P)_G$	gas phase pressure drop (N/m^2)
$(\Delta P)_L$	liquid phase pressure drop (N/m^2)
$(\Delta P)_{LN}$	logarithmic mean partial pressure of CO_2 (N/m^2)
ΔP_{TP}	two-phase pressure drop (N/m^2)
Q	volumetric flow rate (m^3/s)
R	gas constant (J/kmole K)
R_A	rate of reaction (kmol/m^{2}s)
T_0	temperature (K)
U, U'	velocity of fluid and gas–liquid mixture as denoted by subscript (m/s)
U_{mN}	velocity at the nozzle tip (m/s)
V	velocity (m/s)
V_c	volume of contactor (m^3)
w	specific work (work extracted from liquid stream) (W/m)
X	two-phase correlation parameter

Greek symbols

β	pressure recovery ratio $= \Delta p/(\rho_m U_{mN}^2/2)$
ε	hold-up
ε_m	specific energy dissipation (m^2/s^3)
ϕ_G	pressure drop multiplier
γ	specific heat ratio
γ_a	area ratio of throat to entrained fluid inlet
γ_1	area ratio of nozzle to column
γ_2	area ratio of throat to column
γ_3	area ratio of throat to nozzle tip
μ	viscosity (kg/ms)
ρ	density of mixture (kg/m^3)
ρ_e	entrained fluid density (kg/m^3)
ρ_L	liquid density (kg/m^3)

ρ_m	motive fluid density (kg/m^3)
ρ_N	density at nozzle (kg/m^3)
ρ_r	ratio of density of motive fluid to entrained fluid
σ	surface tension (kg/s^2)

Subscripts

atm	atmosphere
C	converging section
Calm	calm section
D	diffuser
e	entrained fluid
ej	ejector
EC	converging section inlet
G	gas
GD	gas at diffuser
GT	gas at throat
in	inlet
L	liquid
LC	liquid at converging section inlet
LT	liquid at throat
m	motive fluid
n, N	at nozzle tip
out	outlet
ON	plane in front of the nozzle
OS	plane in entrained fluid chamber
Spout	spout section
ST	straight tube after diffuser
t, T	throat
0–5	plane at sections with reference to Table 2

ammonia takes place in the presence of KNH_2 as a catalyst. Deuterium is present in gaseous hydrogen as HD at a concentration of about 100 ppm. HD dissolves into the liquid phase and reacts with ammonia to form deuteriated ammonia. The rate of this isotopic exchange reaction in the presence of KNH_2 is very fast as compared to the gas–liquid mass transfer rate (at the temperature and catalyst concentration employed on the industrial scale). The rate of mass transfer, therefore, becomes the controlling step in the overall process. To achieve higher mass transfer rates, on each tray of the exchange towers, a large number of ejectors are provided. The use of ejector trays substantially reduces the size of the column required for the operation.

To design such gas–liquid contactors, it is necessary to establish quantitative relationships between geometry of the ejector, the operating conditions and the performance of the ejector. The important design parameters for such contactors are entrainment rate, pressure drop across the entire length, hold-up of the phases and mass transfer characteristics within the ejector. A majority of the published literature on ejectors deals broadly with the design and performance of steam and liquid-jet ejectors. The reported work on gas–liquid jet ejectors with gas as the motive fluid and liquid as the entrained fluid is scanty. Therefore, studies were undertaken to investigate hydrodynamic and mass trans-

fer characteristics of gas–liquid ejectors with gas as the motive fluid.

2. Previous work

Based on the flow direction, three types of ejectors have been reported, viz., vertical up-flow, vertical down-flow and horizontal flow. Several authors have performed detailed experiments with all the three types of ejectors and have developed numerous correlations to predict the entrainment rate, gas hold-up, mass transfer coefficient and interfacial area, empirically. In the following section, the literature on entrainment rate (in terms of mass ratio), hold-up and mass transfer parameters has been analyzed first. It should be noted that almost all the correlations reported by various authors in the following section employ liquid as primary fluid and gas as secondary fluid.

2.1. Mass ratio

A number of researchers have developed correlations for their respective geometries using dimensional analysis (Table 1). Most of these correlations are similar but vary widely in the exponents of different terms. For example, the exponent of area ratio varies from 0.07 [10] to 0.68 [4]. Bhutada and Pangarkar [10] reported four different correlations, one each for four throats investigated by them. These correlations are highly specific to the nozzle–throat geometry and thus cannot be generalized.

Various authors [4,5,8,11–14] have attempted to predict the entrainment rate based on momentum and energy balances across different sections of the ejector. Table 2 shows the geometry of ejectors and the respective correlations obtained through such analysis as available in literature. All the authors have applied a mechanical energy balance to account for the changes in the cross sectional area of an ejector and a momentum balance across the straight sections of the ejector. The empiricism in their work comes from: (i) fitted loss coefficient, K', (ii) the pressure recovery factor, β and (iii) the correlation between K' and β. From the analysis of the previous work, it can be said that the relationships for mass ratio predictions are semi-empirical and depend on the geometry, fluid property, operating conditions.

Mandal et al. [14] assumed that the entrained gas as ideal and isothermal. The energy loss coefficient across the nozzle was obtained from the energy balance. The pressure energy, kinetic energy and energy dissipation per unit mass of the liquid and gas were considered in the energy balance. No mixing was assumed in throat and diffuser and hence all the energy losses were only the frictional losses. The values of K_{ej} can be back calculated from the ejector efficiency data given by ref. [14]. The values of K_{ej} were in the range 0.06–0.1 for various geometries investigated by the authors. This means that the contributions of the work for the gas compression and the hydrostatic head are very small. Some of the previous models reported by refs. [5,13,14] take the compressibility of air into account. But all these models were developed for liquid as the motive fluid and

Table 1
Mass ratio correlations from dimensionless analysis given by various authors

Primary fluid	Secondary fluid	Geometry and range investigated	Mass ratio correlation	Authors
Air	Water	Flow—upward: $D_N = 0.00808$–0.002676 m, $D_T = 0.0127$ m, $H_T = 0.0889$ m, $(D_N/D_T) = 0.009$–0.2107, $D_C = 0.0635$ m, $H_C = 1.219$ m	$M_r = k \left(\frac{\mu_m}{D_N \rho_m U_m} \right)^{0.76} (A_r)^{0.4} \left(\frac{g\mu_e^4}{\rho_e \sigma_e^3} \right)^{-0.04} \left(\frac{\rho_e - \rho}{\rho_e} \right)^{0.63}$	[7]
Water, glycerine, kerosene	Air	Flow—horizontal: $D_N = 0.0019$–0.00449 m, $D_T = 0.00925$ m, $D_N/D_T = 0.2$–0.48, $H_T = 0$, $D_C = 0.0254$ m, $H_C = 1.1$ m	$M_r = 8.5 \times 10^{-2} \left(\frac{\Delta P}{\rho_e U_e^2} \right)^{-0.3} (A_r)^{0.46} \left(\frac{g\mu_m^4}{\rho_m \sigma_m^3} \right)^{-0.02}$	[8]
Water, glycerine, kerosene	Air	Flow—upward: $D_N = 0.00178$–0.0055 m, $D_T = 0.0127$ m, $H_T = 0.1016$ m, $D_N/D_T = 0.14$–0.433	$M_r = 5.2 \times 10^{-4} \left(\frac{\Delta P}{\rho_e U_e^2} \right)^{-0.305} (A_r)^{0.68} \left(\frac{g\mu_m^4}{\rho_m \sigma_m^3} \right)^{-0.305}$	[4]
Water, mono ethylene glycol	Air	Flow—downward: $D_N = 0.0025$ m, $D_T = 0.005$ m, $H_T = 0.0175$, $D_N/D_T = 0.5$, $H_C = 1$ m, $D_C = 0.01$ m	$M_r = 43.86 \times 10^{-3} \left(\frac{\Delta P}{\rho_e U_e^2} \right)^{-0.38} \left(\frac{g\mu_m^4}{\rho_m \sigma_m^3} \right)^{-0.01}$	[5]
Water	Air	Flow—downward: $D_N = 0.0045, 0.0065$ m, $D_T = 0.018$ m, $D_C = 0.040$ m	$M_r = 2.4 \times 10^{-3} \left(\frac{\Delta P}{\rho_e U_e^2} \right)^{-0.82} \left(\frac{g\mu_m^4}{\rho_m \sigma_m^3} \right)^{-0.01}$	[9]
Water	Air	Flow—downward: $D_N = 0.005, 0.008, 0.01, 0.012$ m, $D_T = 0.016, 0.0159$ m, $D_N/D_T = 1.6$–3.2	$M_r = x \left(\frac{\Delta P}{\rho_e U_e^2} \right)^{y} (A_r)^{z}$; $x = 5.58 \times 10^{-4}$ to 9.67×10^{-4}; $y = -0.135$ to -0.202; $z = 0.07$–0.224	[10]

the gas as the entrained fluid. These models cannot be used directly for the present system where air is the motive fluid.

2.2. Fractional gas hold-up

Table 3 shows the geometry of the ejectors, methods of gas hold-up measurement and the correlations as available in literature. The gas hold-up was correlated to ejector geometry, gas entrainment rate and energy dissipation per unit volume. The form of most of these correlations is similar but with a wide variation in the exponents of different terms. For example, the exponent of gas velocity varies from 0.55 [18] to 1.08 [25]. These correlations are highly specific to particular nozzle–throat geometry.

Zahradnik et al. [2,16,17,19,20] in a series of papers have reported the use of ejector-type gas distributors for the gas–liquid contacting in bubble columns. They have reported that an ejector acts as a gas distributor that allows gas to be entrained into the bubble column rather than sparged. The gas–liquid contact is first achieved in the ejector and subsequently, the flow pattern generated in the bubble column produces good mixing of the gas and the liquid phases. It was reported that for a given superficial gas velocity, higher fractional gas hold-up was observed with the ejector distributor than that with a conventional sieve plate distributor. The gas hold-up was further correlated empirically with the superficial velocity of the gas. The gas hold-up varied linearly with the superficial velocity of the entrained gas, i.e. $\varepsilon_G = 3.47 V_G$, in contrast to less than linear variation of fractional gas hold-up using sieve tray distributor, i.e. $\varepsilon_G = 0.74 V_G^{0.6}$.

Dutta and Raghavan [9] have correlated the gas hold-up in the vessels empirically with the specific power consumption (P/V_L) in the vessel. Bhutada and Pangarkar [10] have stud-

ied the effect of diffuser type on the gas hold-up. Bhutada and Pangarkar [10] have shown that the gas hold-up is a strong function of the gas entrainment rate and a relatively weak function of the geometry of the ejector. They have developed correlation for predicting the gas hold-up for each geometry of the diffuser. Cramers et al. [23] have investigated the effect of the gas density on the gas hold-up in ejector loop reactors. They have observed that the gas hold-up increases with gas density. They too have found a linear relationship between the gas hold-up and the superficial velocity of the entrained gas in agreement with the observations of [16,21,25] have reported the regimes developed and the importance of swirl bodies in the ejector.

All the proposed correlations for the fractional gas hold-up are summarized in Table 3. The fractional gas hold-up is a very strong function of the gas entrainment rate and this is reflected by the correlations proposed [10], which shows, $\varepsilon_G \propto V_G^{0.794}$ and [23], which shows $\varepsilon_G \propto V_G$. The difference in the exponent with respect to power consumption for the two diffusers investigated by ref. [9] is very small.

2.3. Mass transfer characteristics

A number of physiochemical methods have been reported in the literature for the estimation of volumetric mass transfer coefficient $(k_L a)$ of a multiphase contactor. Physical absorption of a solute gas in a liquid, chemical absorption of oxygen in aqueous solutions of sodium sulfite and chemical absorption of carbon dioxide in Na_2CO_3–$NaHCO_3$ solutions are commonly used for the determination of volumetric mass transfer coefficient [9,27]. For the estimation of interfacial area, chemical absorption of oxygen in aqueous sodium sulfite solutions and absorption of CO_2 in aqueous sodium hydroxide solution are

Table 2
Mass ratio correlations from theoretical analysis given by various authors

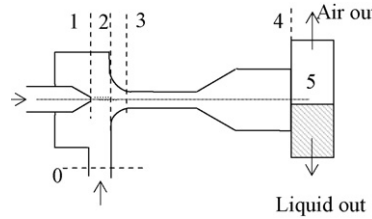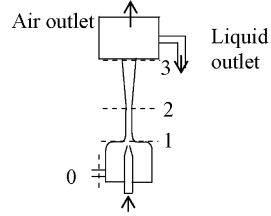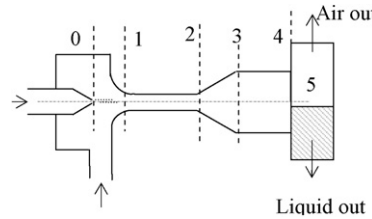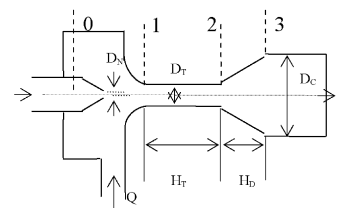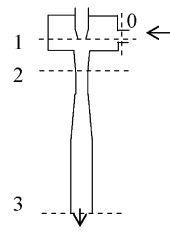| Geometry and range investigated	Geometry and the locations where the energy and momentum balance were taken	Correlation and remarks on loss coefficient	Authors
Flow—horizontal: $D_N = 0.0019$–0.00449, $D_T = 0.00925$, $D_N/D_T = 0.2$–0.48, $H_T = 0$, $D_C = 0.0254$, $H_C = 1.1$.		$M_r^2 \rho_r \left[-\gamma_2^2 + \frac{2\gamma_1 A_r}{(A_r - 1)} + 2(\gamma_1 - 1)\left(\frac{\gamma_3}{\gamma_3 - 1}\right)\left(\gamma_3 - \frac{A_r}{A_r - 1}\right) - \gamma_1^2 \right] -$ $M_r \gamma_1^2 (\rho_r + 1) - (\beta + K')A_r^2 + 2\gamma_1 A_r - (\gamma_1^2 + \gamma_2^2) = 0$	[8]
Primary fluid—water, glycerine and kerosene		All the losses are clubbed as loss factor K' and values of K' were fitted using experimental results K' was empirically fitted to β and A_r $K' = -\beta - 0.0123 A_r + 0.116$ Each area ratio has different K' and the value ranges from 0.01 to 0.06	
Secondary fluid—air maximum L/G = 60			
Flow—upward: $D_N = 0.00178$–0.0055, $D_T = 0.0127$, $H_T = 0.1016$, $D_N/D_T = 0.14$–0.433		$M_r^2 \rho_r \left[\gamma_a^2 + \frac{A_r(A_r - 2)}{(A_r - 1)^2} - 1 \right] - M_r(\rho_r + 1) + 2A_r - (K' + \beta)A_r^2 -$ $1 = 0$	[4]
Primary fluid—water, glycerine, kerosene		All the losses are clubbed as loss factor K' and was fitted to match the experimental values	
Secondary fluid—air		$K' = -0.82\beta + \frac{1.52}{0.95 A_r}$ Each area ratio has different K' and value ranges from 0.01 to 0.28	
Flow—horizontal: $D_N = 0.00278$–0.00798, $D_T = 0.01$, $H_T = 0.06$, $D_N/D_T = 0.278$–0.798, $D_C = 0.0254$.		Total suction was obtained for single phase from loss at each section	[11]
Primary fluid—water, nacl, acetone–water mixture (30%) and glycerol (30%)		Total suction created partially utilized for entrainment and dispersion	

Table 2 (*Continued*)

Geometry and range investigated	Geometry and the locations where the energy and momentum balance were taken	Correlation and remarks on loss coefficient	Authors
Secondary fluid—air Maximum L/G = 14		$M_r^2 =$ $\frac{K_s f_e^n \rho_e}{\rho_m}\left[K'\gamma_3^2 + K'_1\gamma_2^2 + \frac{4f_1 H_T}{D_T} + \frac{4f_2 H_C\gamma_2^2}{D_C} + (1+K_D)(1-\gamma_2)^2\right]$ K_s and n are fitted from experimental data	
Flow—horizontal: review of existing data, single phase		Total loss coefficient = 1 − diffuser efficiency + oss coefficient of throat $P_3 - P_{OS} =$ $\frac{\rho_m}{2}U_m^2\left[\frac{2}{A_r}\left(\frac{M_r^2\rho_r}{A_r-1}+1\right) - \frac{M_r^2\rho_r}{(A_r-1)^2}(1-K_N) - \frac{(1+M_r)(M_r\rho_r+1)}{A_r^2}(1+K_I)\right]$ K_I and K_N were obtained from experimental data of previous authors also single loss coefficient was proposed. Value of K' ranges from 0.21 to 0.34	[12]
Flow—downward: $D_N = 0.0025$, $D_T = 0.005$, $H_T = 0.0175$, $D_N/D_T = 0.5$, $H_C = 1$, $D_C = 0.01$ Primary fluid—water, mono ethylene glycol Secondary fluid—air Maximum L/G = 15		$M_r^2\rho_r\left[\gamma^2\frac{A'_r}{A_r} + \frac{A_r(A'_r-2)}{(A'_r-1)^2}\right] + 2A_r + \frac{1+M_r}{M_r\rho_r(1+\varepsilon)+1} + [2A_r^2 Fr - M_r\rho_r(1+\varepsilon)+1] - (K''+\beta)A_r^2 = 0$ $K' = \leftrightharpoons - 1.11\beta + 0.445$ All the losses are clubbed as loss factor K' and was fitted with experimental values. Values of K' ranges from 3–7	[5]

Table 3
Hold-up, $k_L a$ and a measurement methods and correlations given by various authors

System	Dimensions (m)	Q_G (m³/s)	Q_L (m³/s)	Method of measurement			Correlation	Author
				Hold-up	$k_L a$	a		
Upward, primary—water; secondary—air	$D_N = 0.006$–0.016, $D_T = 0.01$–0.028, $H_T = 0.05$–0.26	5×10^{-5} to 1.3×10^{-3}	0 to 6.6×10^{-4}	2, 3			$\frac{\varepsilon_G}{\varepsilon_{G0}} = 0.5\left(\frac{D_N}{D_T}\right)^{-0.3} Fr^{0.3}$, $\varepsilon_{G0} = 0.38 U_G^{*0.84}$, $U_G^* = \frac{U_G}{[\Delta P g \sigma / \rho_L^2]^{1/4}}$	[15]
Upward, primary—water; secondary—air	Type 1: $D_N = 0.006$–0.011, $L = 0.025$ Type 2: $D_N = 0.006$, $L = 0.007$ Type 3: $D_N = 0.008$, $L = 0.0015$, $D_T = 0$, $H_T = 0$, $D_{Dinlet} = 0.0638$, $D_{Doutlet} = 0.159$, $H_D = 0.43$, $D_C = 0.292$	0.28×10^{-3} to 5.04×10^{-3}	0.5×10^{-3} to 2×10^{-3}	1	1		$\varepsilon_G = 0.05 e_D^{0.69}$ $e_D = \frac{\Delta P Q_L}{V_L \rho_L}$ $k_L a = 0.04 e_D^{0.54}$	[16]
Upward, primary—water; secondary—air	$D_N = 0.006$–0.010, $D_C = 0.292$	0.28×10^{-3} to 4.48×10^{-3}, 0.004–0.067 m/s	5.5×10^{-4} to 1.8×10^{-3} m³/s	1	1		$\varepsilon_G = 3.47 U_G$, $k_L a = 2 U_G$	[17]
Upward, primary—water; secondary—air	$D_N = 0.008$, $D_T = 0.01$, $H_T = 0.225$, $D_C = 0.15$, $H_C = 1.795$	0–1×10^{-3} m³/s	0–6.67×10^{-4} m³/s	2, 4	2	1	$\varepsilon_{G,S_{Pout}} = 0.346 U_G^{0.55} Fr^{0.3}$, $\varepsilon_{G,Calm} = 0.346 U_G^{0.55} Fr^{0.3}$, $0.472 \times 10^{-2} < U_G < 5.6 \times 10^{-2}$ m/s, $D_B = 1.213 \times 10^{-2} U_G^{0.2} Fr^{-0.375}$, $k_L a_{S_{Pout}} = 8.42 \times 10^{-2} U_G^{0.6} Fr^{1.0}$, $k_L a_{Calm} = 0.329 U_G^{0.75} Fr^{0.55}$, $a_{S_{Pout}} = 0.285 U_G^{0.36} Fr^{0.8}$, $a_{Calm} = 0.249 U_G^{0.6} Fr^{0.65}$	[18]
Upward, primary—water; secondary—air	$D_N = 0.008$, L $= 0.025$, 0.007, 0.0015, $D_{Din} = 0.016$, $D_{Dout} = 0.04$ and 0.028, $H_D = 0.1$–0.4, $D_C = 0.3$ m	8.3×10^{-4} to 7.7×10^{-3} m³/s, superficial velocity 0.013–0.107 m/s	5.5×10^{-4} to 1.8×10^{-3} m³/s	1	1		$\varepsilon_G = 0.057 e_D^n$, $n = 0.53$ (for $H_D = 0.4$), $n = 0.42$ (for $H_D = 0.2$), $n = 0.35$ (for $H_D = 0.1$), $k_L a = 0.036 e_D^{0.54}$	[19]
Upward, primary—water; secondary—air							$k_L a = 0.7 \varepsilon_G^{1.05}$	[20]
Downward, primary—water; secondary—air	$D_N = 0.005$, 0.008, 0.01, 0.012 m, $D_T = 0.016$, 0.0159 m, $D_N/D_T = 1.6$–3.2	6.4×10^{-4} to 3.2×10^{-3} m³/s	4×10^{-4} to 2.8×10^{-3}	1			$\varepsilon_G = A(Q_G)^B$, $A = 0.94$–2.66, $B = 0.74$–1.54	[10]
Downward, primary—solution of $NaHCO_3$ and Na_2CO_3; secondary—air + CO_2 mixture	$D_N = 0.0045$, 0.0065 m, $D_T = 0.018$ m, $D_C = 0.040$ m.	0.5×10^{-4} to 3.0×10^{-3}	1×10^{-4} to 5×10^{-4}		3	2	$k_L a = 0.044 \left(\frac{P}{V}\right)^{0.76}$	[9]
Upward, primary—sodium sulfite solution, secondary—air	$D_N = 0.003$–0.02, $D_T = 0.01$–0.03, $H_T = 0.05$–1.25	0.25×10^{-3} to 1×10^{-4}	0.3×10^{-3} to 4×10^{-3}		2	1	$a_{S_{Pout}} = 15,000 \varepsilon^{1.2}$, $a_{Calm} = 7500 \varepsilon_G^{1.1}$	[21]
Downward, primary—water; secondary—air	$D_N = 0.004$–0.006, $D_T = 0.012$, $D_D = 0.04$	0.9×10^{-4} to 0.24×10^{-2}	0.3×10^{-3} to 0.8×10^{-3}	1			$\frac{k_L a V_{ej}^{1/3}}{D_C} = 5.4 \times 10^{-4} Re^2 \frac{G}{G+L}$, $1.3 < \frac{G}{L} < 3$, $\frac{k_L a V_{ej}^{1/3}}{D_C} = 3.1 \times 10^{-4} Re^2$	[22]
Downward, primary—water; secondary—air	Not mentioned	0–7×10^{-3}	2.8×10^{-4} to 2×10^{-3}	1			$\varepsilon_G = 7.7 U_G \left(\frac{\rho_G}{\rho_L}\right)^{0.11}$	[23]
Downward, primary—water; secondary—air	$D_N = 0.009$	2.22×10^{-4} to 3.36×10^{-3}	5.56×10^{-4} to 2.22×10^{-3}			1	$a = 19,500 \left(\frac{P}{V}\right)^{0.4} \varepsilon_G (1-\varepsilon_G)^{0.4}$	[24]
Upward, primary—water; secondary—air	$D_N = 0.006$–0.012, $D_T = 0.016$, $D_{out} = 0.04$	2.78×10^{-4} to 5.1×10^{-3}	5.5×10^{-4} to 2×10^{-3}	2			$\varepsilon_G = 2.81 U_G^{0.9}$	[2]
Upward, primary—water; secondary—air	$D_N = 0.01$, $D_T = 0.018$, $H_T = 0$–0.36	0–2.33×10^{-3}	0–0.083 m/s	2			$\frac{\varepsilon_G}{1-\varepsilon_G} = 5.91 U_G^{1.08} e_D^{0.03}$	[25]
Downward, primary—water; secondary—air	$D_N = 0.004$, 0.0047 and 0.0053, $D_T = 0.012$, $H_T = 0.024$–0.120	$Q_G/Q_L = 0$–1.5	Not mentioned	1			$k_L a = C e_D^{0.65} \varepsilon_G^* \left(\frac{\rho_L^2 \rho_G}{\sigma^3}\right)^{0.2} \left(\frac{H_T}{D_T}\right)^{0.42} \left[1 - 0.55\left(0.38 - \frac{D_N}{D_T}\right)^2\right]$	[1]

S. Balamurugan et al. / Chemical Engineering Journal 131 (2007) 83–103

Table 3 (*Continued*)

System	Dimensions (m)	Q_G (m³/s)	Q_L (m³/s)	Method of measurement			Correlation	Author
				Hold-up	$k_L a$	a		
Downward, primary—water, CMC; secondary—air	$D_N = 0.004–0.008$, $D_T = 0.019$, $H_T = 0.184$, $H_D = 0.204$, $D_C = 0.0156$	1.11×10^{-6} to 1.89×10^{-5}	9.56×10^{-6} to 2.75×10^{-5}	2			$\varepsilon_G = 0.365 Re^{-0.164} \left(\dfrac{g\mu^4}{\rho\sigma^3}\right)^{-0.029} A_r^{0.032} H_T^{0.207}$	[26]
Downward, primary—water; secondary—air	$D_N = 0.004–0.008$, $D_T = 0.019$, $H_T = 0.184$, $H_D = 0.204$	0.83×10^{-4} to 1.58×10^{-3}	0.98×10^{-4} to 2.63×10^{-4}		3	2	$k_L a = 1.08 U_G^{0.92}$, $a = 0.38 \times 10^4 U_G$	[27]

Hold-up measurement methods: 1. Bed expansion method; 2. difference of static pressure along the column; 3. spark photography for bubble size estimation; 4. photography for bubble size estimation.
Mass transfer estimation measurement methods: 1. Dynamic method—monitoring of unsteady oxygen absorption into previously deoxygenized water in the bed, i.e. on the evaluation of system response to an input step change nitrogen–air; 2. O₂ absorption in sodium sulfite solution with Cobaltous sulfate as catalyst; 3. absorption of lean CO₂ in the mixture of NaHCO₃ and Na₂CO₃.
Interfacial area measurement methods: 1. O₂ absorption in sodium sulfite solution with Cobaltous sulfate as catalyst; 2. absorption of CO₂ in aqueous solution of sodium hydroxide.

the commonly used systems. Table 3 shows the geometry of ejectors used, methods of mass transfer coefficient ($k_L a$) and interfacial area (a) measurements and the correlations obtained by previous authors.

Zahradnik et al. [17] has shown that the mass transfer coefficient in a bubble column operated with an ejector gas distributor increased linearly with the superficial velocity of the entrained gas ($k_L a = 2.0 V_G$). However, the mass transfer characteristics for a conventional bubble column operated with a sieve plate distributor can be correlated as $k_L a = 0.75 V_G^{0.85}$. It has been reported that the comparison of the two distributors shows that for the same mass flow rate, the ejector distributor gives higher mass transfer coefficients. Moresi et al. [28] investigated the performance of a fermentor operated with an ejector. They have correlated the values of mass transfer coefficient empirically with the power consumption per unit mass of the liquid. The values of mass transfer coefficient with 6 and 4 mm diameter nozzles were not significantly different. Dutta and Raghavan [9] have empirically correlated the values of mass transfer coefficients in ejector loop reactors with the power consumption per unit volume of the reactor.

Dirix and van der Wiele [22] have shown that there are two regimes in the ejectors namely the bubble (froth) flow regime and jet flow regime. In the bubble (froth) flow regime, the mass transfer coefficient depends on gas and liquid flow rates and also Reynolds' number (calculated from the fluid properties at the nozzle tip), whereas, in the jet flow regime it depends only on the nozzle Reynolds' number.

Cramers et al. [23] have correlated the interfacial area with the jet power and the gas velocity. They have reported that the liquid height in the holding tank affects the mass transfer characteristics of the ejector significantly. The overall specific interfacial area increases with both the gas and liquid flow rates. At the lower gas flow rates, the gas holdup and the specific interfacial area are almost proportional to the superficial gas velocity. For the higher liquid flow rates, this linear dependency vanishes abruptly caused by the change in the flow regime. It was shown by these authors that the ratio of D_N/D_T has a significant effect on the local energy dissipation rate within the mixing zone and consequently on the local k_L and a values. An optimum value of interfacial area was obtained for D_N/D_T of 0.4. Cramers and Beenackers [1] have reported a correlation for interfacial area as a function of the gas and liquid physical properties, specific power input and the gas hold-up.

The reported correlations for volumetric mass transfer coefficients and interfacial area appear to depend significantly on the geometry of the ejector and power input per unit volume. It is worth to re-emphasize that all these correlations were developed for liquid as the motive fluid and gas as the entrained fluid. These models cannot be directly used for the present system where air is the motive fluid.

Since the literature of ejectors with gas as a motive fluid is scanty, it was thought desirable to investigate the hydrodynamic and mass transfer characteristics of ejectors with air as a primary fluid (to characterize the performance of ejector trays as mentioned at the end of Section 1) with the help of detailed experiments.
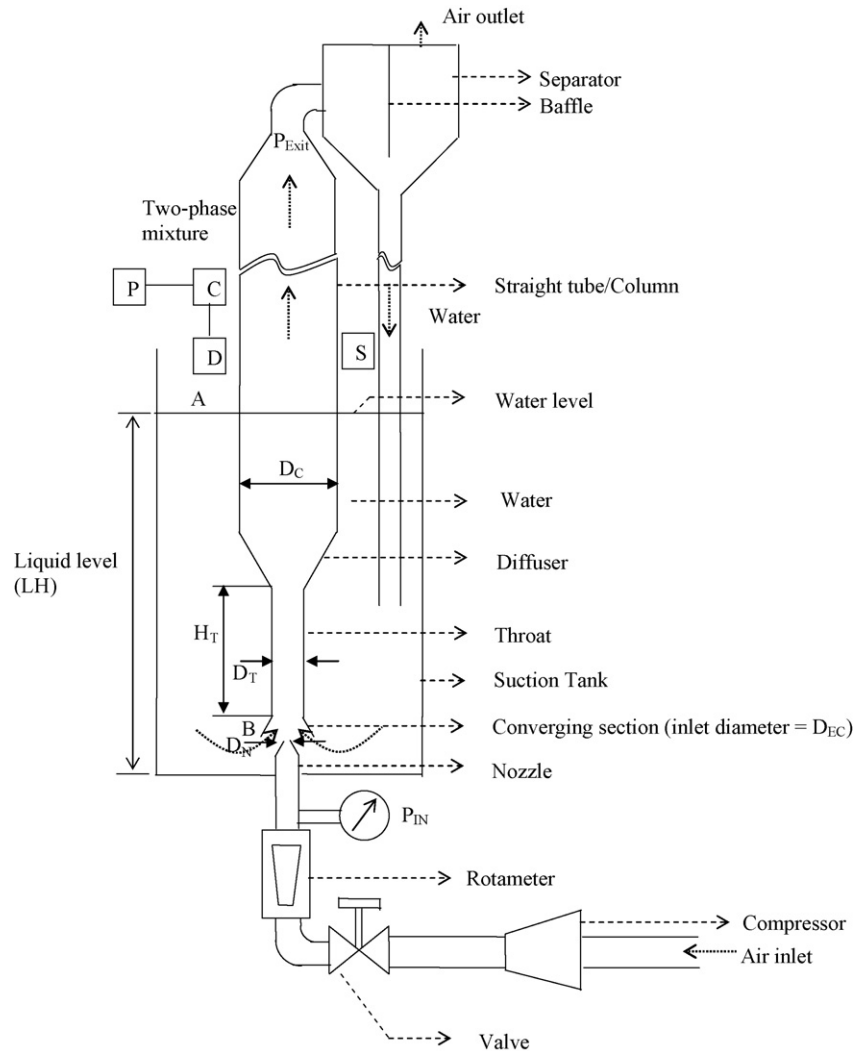
Fig. 1. Gas–liquid ejector experimental apparatus for measuring liquid entrainment. (A) Liquid surface; (B) nozzle tip; (C) data acquisition facility; (D) detector; P, personal computer; S, Source.

3. Experimental setup and methodology

3.1. Liquid entrainment rate

A schematic diagram of the experimental setup is shown in Fig. 1 with air as the motive fluid and water as the entrained fluid. The experiments were carried out in an acrylic column of 0.06 m in diameter and 1 m in height. The air flow rate was manually controlled with the help of a calibrated rotameter. The air pressure just before the entry into the nozzle was measured using a digital pressure gauge (AZ Instrument make with accuracy of 0.3%). The entrainment rate of the liquid was measured by manually collecting the liquid from the gas–liquid separation tank in a known period. The ratio of the entrained water to the amount of air is called as entrainment ratio (kg of entrained water carried per kg of air). The velocity of air flowing through the nozzle was varied over a wide range (50–250 m/s). The corresponding entrainment rate and corresponding pressure drop were measured for each air flow rate. Table 4 shows various geometry parameters that were investigated.

3.2. Fractional gas hold-up

The γ-ray attenuation technique using a pencil beam was used for the determination of fractional gas hold-up. The system (Fig. 1) consists of a 67.5 μC 137Cs γ-source (disk source of 0.02 m diameter), sodium iodide with thallium-activated scin-

Table 4
Dimensions of the ejector and parameters varied in the experiments

Parameter	Values
Nozzle inlet diameter, D_0 (m)	0.0254
Nozzle diameter, D_N (m)	0.004, 0.006, 0.008, 0.01, 0.012
Throat diameter, D_T (m)	0.02, 0.0254, 0.04
Throat height, H_T (m)	0.05, 0.1
Converging section diameter (m)	0.05
Column diameter, D_C (m)	0.06
Column height (m)	1
Water level in the suction tank, LH (m)	0.25, 0.3, 0.35, 0.4, 0.45, 0.5
Pressure (N/m^2, g)	1013–114,000
Air flow rate (m^3/s)	0.0026–0.026

tillation detectors (Bicron), photomultiplier tube, preamplifier, multichannel (eight channels) analyzer, data acquisition system, and related hardware and software. The source collimator slit was 0.03 m long and 0.003 m in wide. Collimators for the detectors are cylindrical 0.087 m in diameter and 0.103 m long. The collimator slit of detector was 0.035 m in length and 0.004 m in width. The experimental procedure used here was similar to that used by refs. [29,30]. Pencil beam measurements were carried out at the centre of the column at a height of 0.6 m from the nozzle tip. Trial runs indicated that a dwell time of around 5 s and 100 events were necessary to obtain reproducible values of intensity. The total acquisition time for each line plane (chord) measurement was therefore 500 s. For the above-mentioned conditions, water counts (column full of liquid) and air counts (column completely empty) were taken. Two-phase counts were taken for various nozzle velocities and different liquid levels. The chordal hold-ups were calculated using the following equation:

$$\varepsilon_G = \frac{\ln(I_{TP}/I_L)}{\ln(I_G/I_L)} \tag{1}$$

where I_{TP}, I_L and I_G are gamma ray intensities in a two-phase, column filled with liquid only and empty column, respectively.

3.3. Volumetric mass transfer coefficient ($k_L a$)

For the determination of $k_L a$, absorption of lean CO_2 (A) in aq. buffer solutions of Na_2CO_3–$NaHCO_3$ (B) is used for this purpose. The absorption process is accompanied by a chemical reaction (Eq. (2)).

$$CO_2 + Na_2CO_3 + H_2O \rightarrow 2NaCHO_3 \tag{2}$$

Doraiswamy and Sharma [31] have given an expression for the rate of mass transfer per unit volume of the reactor for a reaction fast enough to reduce concentration of CO_2 in the bulk liquid to zero

$$R_A a = k_L a [[CO_2^*] - [CO_2]_0] \tag{3}$$

$$R_A a = k_L a [CO_2^*] \tag{4}$$

The conditions for no reaction to occur in the diffusion film, are given by Eqs. (5) and (6)

$$k_L a \ll l k_2 [Na_2CO_3]_0 \tag{5}$$

$$\sqrt{M} = \sqrt{\frac{D_{CO_2} k_2 [Na_2CO_3]_0}{k_L^2}} < 1 \tag{6}$$

A mixture of 1:20 of CO_2 and air was passed into the ejector setup (Fig. 1) for a particular nozzle diameter, throat diameter of 0.0254 m, throat height of 0.1 m. A mixture of Na_2CO_3–$NaHCO_3$ was filled up to the desired liquid level in the suction chamber. The rate of reaction of CO_2 with Na_2CO_3 was estimated through the rate of formation of $NaHCO_3$. Samples were taken at regular intervals of time to estimate the concentration of $NaHCO_3$ present.

The rate of absorption of CO_2 was estimated from the amount of sodium bicarbonate formed with time. Rate of CO_2 consump-

tion was estimated using the following equation

$$\text{rate of } CO_2 \text{ consumption} = \frac{\text{rate of formation of } NaHCO_3}{2} \tag{7}$$

The solubility of CO_2 was estimated using the Henry's constant (corrected for temperature and ionic strength) and logarithmic mean partial pressure of CO_2 as shown below.

$$[CO_2^*] = H \times (\Delta P)_{LN} \tag{8}$$

The mean partial pressure of CO_2 at the inlet and at the outlet were estimated using the following equations:

$$PP_{CO_2 \text{ in}} = \left(\frac{Q_{CO_2 \text{ in}}}{Q_{CO_2 \text{ in}} + Q_{\text{air in}}} \right) \times P_{\text{in}} \tag{9}$$

$$PP_{CO_2 \text{ out}} = \left(\frac{Q_{CO_2 \text{ out}}}{Q_{CO_2 \text{ out}} + Q_{\text{air out}}} \right) \times P_{\text{out}} \tag{10}$$

The overall mass transfer coefficient ($k_L a$), was estimated using Eq. (4) from the estimated values of the rate of absorption and solubility of CO_2 in the aqueous buffer solutions. The same procedure was followed for different gas velocities and nozzle diameters.

3.4. Interfacial area (a)

For the measurement of effective interfacial area (*a*), 1:20 CO_2–air mixture was absorbed in aqueous sodium hydroxide solutions. The pertinent details of the above system are given by refs. [31–33]. The reaction between a gaseous solute CO_2 and aqueous reactant NaOH is so fast that it reacts completely in the diffusion film and no free CO_2 exists in the bulk of NaOH. The reaction rate is slow enough that no depletion of NaOH occurs in the film, and then the rate of transfer of CO_2 can be given by:

$$R_A a = [CO_2^*] a \sqrt{D_{CO_2} k_2 [NaOH]_0} \tag{11}$$

The conditions to be satisfied for the fast reaction regime and complete reaction of CO_2 in the diffusion films without causing significant drop in concentration of NaOH in the diffusion film are given as:

$$\sqrt{M} = \sqrt{\frac{D_{CO} k_2 [NaOH]_0}{k_L^2}} \gg 1 \tag{12}$$

$$\sqrt{M} \ll \frac{[NaOH]_0}{2[CO_2^*]} \left[\frac{D_{NaOH}}{D_{CO_2}} \right] \tag{13}$$

For each gas flow rate, at one particular liquid level of NaOH in the suction chamber, the CO_2–air mixture was passed through the ejector. The gas flow rates maintained were the same as those used in the $k_L a$ measurements. Eq. (14) shows the reaction that takes place during this process

$$CO_2 + 2NaOH \rightarrow Na_2CO_3 + H_2O \tag{14}$$

Samples were drawn at regular intervals of time and the unreacted NaOH was determined using standardized HCl solutions.

The rate of absorption of CO_2 was estimated from the rate of consumption of NaOH with time as given below:

$$R_A a = \frac{[NaOH]_{reacted\ in\ suction\ tank}}{2 \times ejector\ volume \times time} \tag{15}$$

The solubility of CO_2 in NaOH was estimated using the similar procedure explained in the previous section. Knowing the rate of absorption and CO_2 solubility in aq. NaOH solution, the interfacial area was estimated using Eq. (11). The values of diffusivity of CO_2 in aqueous NaOH and second order rate constant were taken as 1.96×10^{-9} m²/s and 2×10^4 m³/(s kmol), respectively [31]. The same procedure was followed for all the other gas velocities and nozzle diameters.

The true mass transfer coefficient k_L was estimated from experimental values of $k_L a$ and a.

4. Analysis of performance of ejectors

4.1. Semi-empirical model

As a first step, the correlations reported by previous authors (Table 1), were tested for their predictive capability. However, these correlations were unable to predict the entrainment ratio. This is because of the differences in the geometry (throat diameter, nozzle diameter, etc.) and the operating conditions (motive fluid, motive fluid velocities, etc.). Therefore, it was thought desirable to develop a semi-empirical model to predict the liquid entrainment rate taking into account: (i) the compressible nature of air in the nozzle, (ii) pressure drop for two-phase flow and (iii) the losses due to change in cross sectional area.

The measured variables in the experiment are the liquid entrainment rate, the pressure at the inlet of the nozzle and gas volumetric flow rate and mass flux at the nozzle inlet. This experimental information was used to estimate the model constants. The model algorithm is explained with the help of a flow chart shown in Fig. 2 and the procedure is described below in detail:

(1) The gas phase compressibility effects are important when gas is the motive fluid. Also, the major effect of the gas compressibility is in the nozzle where the gas flow occurs across a very large change in the cross sectional area. Lapple [34] reported a chart obtained from the solution of simultaneous differential equations (integration of the differential forms of the continuity, momentum and total energy equations for an ideal gas, assuming constant friction factor). This chart gives the gas discharge from a large chamber through an isentropic nozzle followed by a duct. It was assumed that the sonic velocity in a gas flowing through a pipe depend on the condition of flow. The condition may be isothermal or adiabatic. This was modified by ref. [35] considering that the velocity propagation of a sonic wave is independent of the type of flow. Also, the sonic condition can exist only at pipe exit. Hence, the Lapple charts were corrected by ref. [35] for the case of an isentropic nozzle followed by adiabatic pipe flow.

The mass flux during the choked condition was estimated from pressure measured at the nozzle inlet, P_{in} using the following equation:

$$G^* = P_{in}\sqrt{\frac{M\gamma}{RT_0}\left(\frac{2}{\gamma+1}\right)^{\gamma+1/\gamma-1}} \tag{16}$$

Levenspiel [35] reported the graphical relationship between mass flux ratio (G/G^*) and the pressure ratio (P_N/P_{in}). This graphical relationship was used to estimate the pressure at the nozzle tip, P_N. The curve corresponding to resistance parameter $N = 0$ ($N = 4fL_T/D_H$, this is because there is no straight pipe after the nozzle) in the graph has been represented by the following equation:

$$\frac{G}{G^*} = -7.51\left(\frac{P_N}{P_{in}}\right)^2 + 9.93\left(\frac{P_N}{P_{in}}\right) - 2.31 \tag{17}$$

The value of G^* used in Eq. (17) was estimated from Eq. (16), G (air mass flux) and P_{in} was experimentally measured. Hence, Eq. (17) was solved for P_N to estimate the pressure at nozzle tip.

(2) The amount of liquid entrained depends on the amount of suction created by air jet due to the pressure reduction at the nozzle tip. A mechanical energy balance was applied between the liquid surface (open to atmosphere) and the nozzle tip (Fig. 1). The hydrostatic head between the liquid surface and the nozzle tip acts as the driving force for the liquid entrainment. The loss in the mechanical energy due to changes in the direction of the entrained liquid are expressed as a head loss coefficient K' in the following manner:

$$\frac{P_{atm}}{\rho_L} + gh = \frac{P_N}{\rho_L} + \frac{1}{2}K'V_{LC}^2 \tag{18}$$

The distance between the nozzle tip and the liquid surface is h. K' was the unknown in Eq. (18). The value of K' was fitted such that the predicted liquid entrainment rate (calculated from V_{LC} in Eq. (18), where V_{LC} is the velocity of liquid at the entry of ejector) match the experimentally measured entrainment rate (Q_L). Fig. 3 shows the parity plot of measured liquid entrainment rate and the predicted entrainment rate. It can be seen that the predicted values of entrainment rate are in good agreement with the experimental measurements. The liquid entrainment rate predicted from Eq. (18) and air mass flow rate measured were used for the two-phase pressure drop predictions.

(3) The pressure at the ejector outlet, P_{out} is open to atmosphere and hence the two-phase pressure drop can be estimated from the following equation.

$$(\Delta P)_{TP} = P_{out} - P_N \tag{19}$$

The procedure used to estimate the two-phase pressure drop from the individual pressure drops of gas and liquid is given in the Step 4.

(4) The frictional pressure drop associated with two-phase gas–liquid flow is higher than that obtained if either of the

Measured variables in experiment: $P_{IN(M)}$, Gas mass flux (G), $Q_{L(M)}$, $P_{OUT(M)}$ (1 atm)
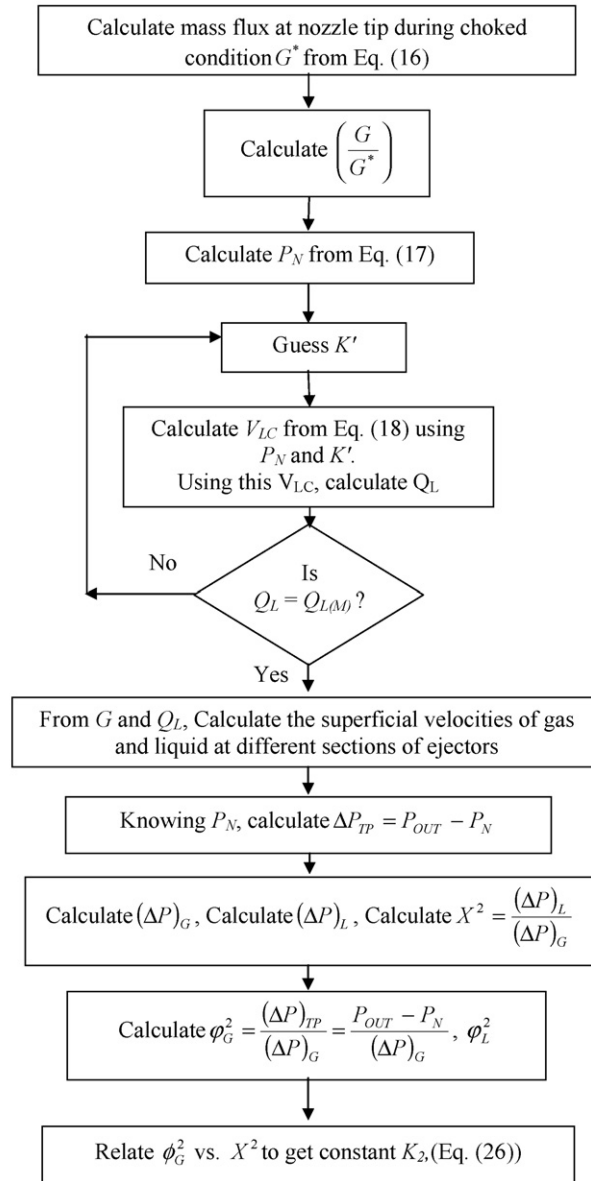

Fig. 2. Flow chart indicating the stepwise procedure to predict the entrainment rate.

two phases were flowing along through the same channel at the total mass flow rate. This higher pressure drop is due to the energy losses from the interactions between liquid phase and gas phase since the gas phase velocity is higher than that of liquid and the reduced effective area of the gas flow due to the presence of two phases flowing simultaneously [36]. To get the two-phase pressure drop, the individual single-phase pressure drops of air $(\Delta P)_G$ and water $(\Delta P)_L$ in the ejector tube were estimated. The gas side pressure drop $(\Delta P)_G$ across the ejector was estimated as if only air flowed through the ejector. Similarly, the liquid side pressure drop $(\Delta P)_L$ was estimated as if only water flowed through the ejector. The ejector system, where two-phase flow occurs was divided into different sections, namely: (i) convergent section just after nozzle exit, (ii) throat, (iii) diffuser (diver-

gent section) and (iv) straight tube. The two-phase nature of flow in all these sections is complex. Further the changes in compressibility are no longer significant as this is not a single-phase but a two-phase flow, where one phase is dispersed in the other. In order to model the energy loss in the converging and the diverging sections, head loss coefficients were calculated based on the changes in the cross sectional area. The pressure losses that are occurring in the converging and diverging section are primarily due to the changes in the cross sectional area. The convergent section loss coefficient was obtained from following equation:

$$K_C = 0.4 \left[1 - \left(\frac{D_T^2}{D_{EC}^2} \right) \right]^2 \tag{20}$$
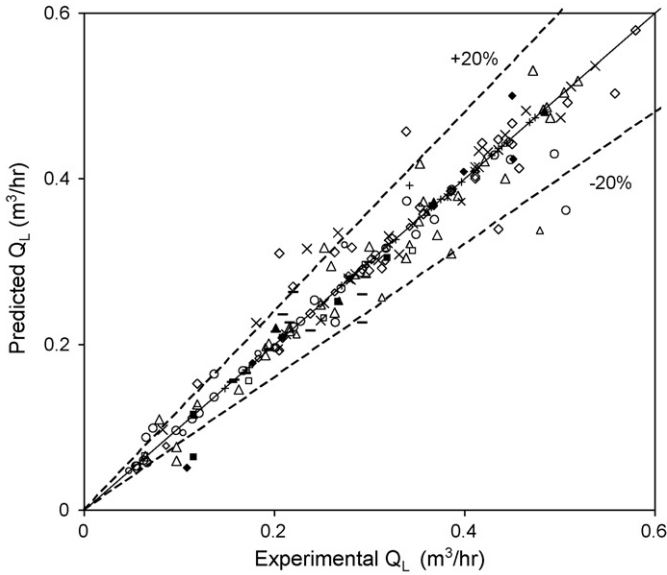
Fig. 3. Parity plot between experimental and predicted entrainment rate. For a constant throat diameter, $D_T = 0.0254$ m; throat height, $H_T = 0.1$ m; nozzle diameter, $D_N = 0.004$ m; liquid level (L) are: (■) $L = 0.4$ m, (♦) $L = 0.45$ m, (▲) $L = 0.5$ m. For $D_N = 0.006$ m, liquid level (L) are (○) $L = 0.25$ m, (□) $L = 0.3$ m, (◇) $L = 0.35$ m, (△) $L = 0.4$ m, (×) $L = 0.45$ m, (–) $L = 0.5$ m. The following cases are for all the liquid levels (i.e., L = 0.25, 0.3, 0.35, 0.4, 0.45, 0.5 m), (×) $D_N = 0.008$ m, (+) $D_N = 0.010$ m, (—) $D_N = 0.010$ m. For a constant throat diameter, $D_N = 0.006$ m, $H_T = 0.05$ m, (△) $D_T = 0.2$ m, (◇) $D_T = 0.0254$ m, (○) $D_T = 0.04$ m.

While the diffuser section loss coefficient was obtained from the equation given below:

$$K_D = \left[1 - \left(\frac{D_T^2}{D_C^2} \right) \right]^2 \tag{21}$$

Thus, these head loss coefficients would be different depending upon the ejector geometry and are not assumed to be constant. The values of the head loss coefficients are in the range 0.05–0.28 for the converging section and 0.31–0.79 for the diverging section for various throat diameters.

The pressure drops across the converging and diverging sections were estimated using their corresponding loss coefficients. The pressure drop of liquid across the converging section was estimated using the following equation:

$$(\Delta P)_{LC} = \frac{1}{2} K_D \rho_L V_{LC}^2 \tag{22}$$

Similarly, the pressure drop of air across the converging section was estimated using the velocity of air at converging section inlet and density of air. Similar procedure was used to estimate the pressure drop of both water and air across the diverging section, i.e. $(\Delta P)_{LD}$ and $(\Delta P)_{GS}$, respectively.

The procedure for estimating the two-phase pressure drop in throat and straight tube is explained in the following section. The frictional pressure drop of water in the throat was estimated from Eq. (23) with friction factor f_L, calculated from the standard

correlation applicable for turbulent condition.

$$(\Delta P)_{LT} = \frac{2 f_L \rho_L H_T V_{LT}^2}{D_T} \tag{23}$$

The pressure drop of water in the column $(\Delta P)_{LS}$ was estimated in a similar manner and the total pressure drop in liquid side $(\Delta P)_L$ was estimated by adding all the liquid side pressure drops, i.e. $(\Delta P)_{LC}$ (converging section), $(\Delta P)_{LT}$ (throat), $(\Delta P)_{LD}$ (diffuser) and $(\Delta P)_{LS}$ (straight tube section). Similarly, total pressure drop at the gas side $(\Delta P)_G$ was estimated using the gas properties and corresponding velocities which were in the turbulent regime. With the individual pressure drops in all the sections, the parameter X^2 was obtained from equation below:

$$X^2 = \frac{(\Delta P)_L}{(\Delta P)_G} \tag{24}$$

The two-phase parameter ϕ_G^2 was defined using Eq. (25). The two-phase pressure drop $(\Delta P)_{TP}$ across the ejector indicates the overall pressure drop across the ejector due to the two-phase flow. It is the pressure drop between nozzle exit (P_N) and ejector outlet (P_{out}, 1 atm).

$$\phi_G^2 = \frac{(\Delta P)_{TP}}{(\Delta P)_G} \tag{25}$$

where the two-phase parameter ϕ_G^2 was related as a linear function of the parameter X as given in Eq. (26).

$$\phi_G^2 = K_2 X^2 \tag{26}$$

The value of two-phase parameter, K_2 was adjusted so that the P_{out} estimated is 1 atm. The value of K_2 (Eq. (26)) was found to be equal to eight and independent of nozzle diameter, throat diameter, throat height, gas velocity and liquid level. The correlations discussed in the previous work section were found to be a strong function of the ejector geometry.

The loss coefficient K' (Eq. (18)) was found to be dependent on the area ratio (throat area to the nozzle area) and was independent of the gas velocity and the liquid level. The ratio of the throat area to the nozzle area decides the extent of change in direction of the entrained liquid. Also, the K' values obtained are comparable with the previously reported values. The correlation obtained through power law fit with R^2 (regression coefficient) of 0.98 is given below.

$$K' = 1.6 \left(\frac{A_T}{A_N} \right)^{-1.2} \tag{27}$$

Since the data used for this prediction indicated wide variation in the geometrical parameters such as nozzle diameter, throat diameter and throat height and operating parameters such as liquid level and gas velocities, this model can be used to predict the liquid entrainment rate knowing the loss coefficient K'.

4.2. Effect of nozzle velocity, liquid level and area ratio on entrainment rate

The effect of gas velocity, liquid level and geometry on the performance of the ejector has been studied in detail in this section. The pressure at the nozzle tip (P_N) predicted from the model and the two-phase pressure drops in the ejector (convergent section, throat, diffuser and the straight tube column) estimated from the correlation were used to analyze the performance of the ejector.

Fig. 4A shows the effect of velocity of air at the nozzle tip on experimentally measured liquid entrainment rates for different liquid levels in the suction tank. The liquid entrainment rate increases with the nozzle velocity. But at higher nozzle velocity,

(A)

(B)
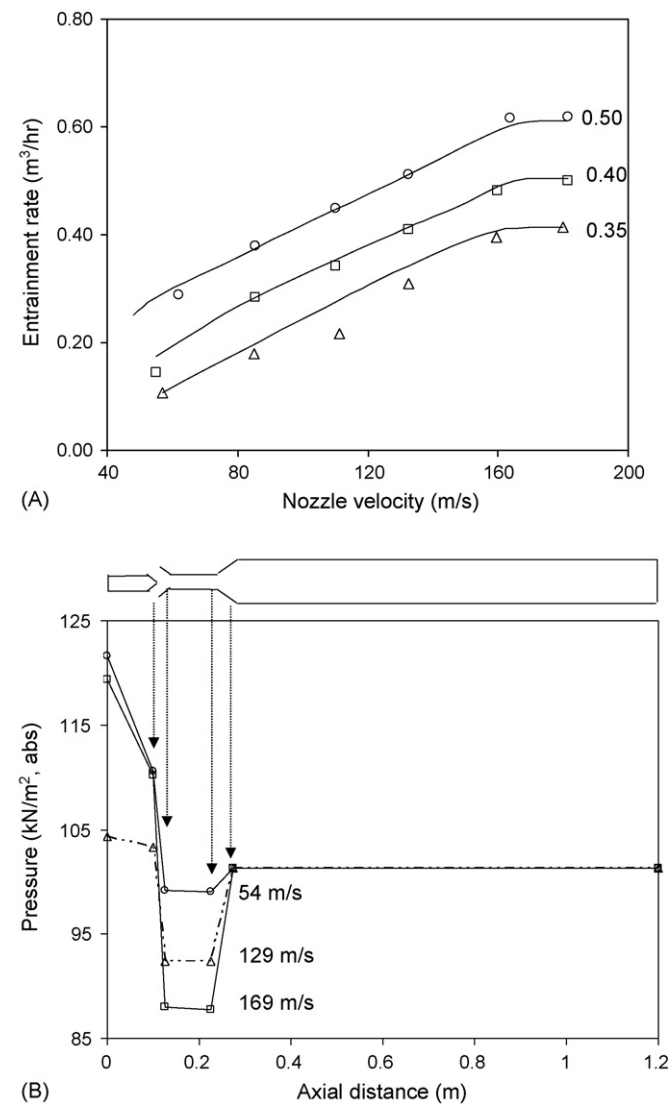
Fig. 4. (A) Effect of nozzle velocity on measured entrainment rate for $D_N = 0.008$ m, $H_T = 0.1$ m and $D_T = 0.0254$ m. ($\triangle$) Liquid level = 0.35 m, ($\square$) liquid level = 0.40 m, ($\bigcirc$) liquid level = 0.50 m, (—) entrainment rate predicted from model. (B) Effect of nozzle velocity on pressure profile from the centre line of ejector with the axial locations from the nozzle inlet for $D_N = 0.008$ m, $D_T = 0.0254$ m, LH = 0.50 m. ($\bigcirc$) $V_N = 54$ m/s, ($\triangle$) $V_N = 129$ m/s, ($\square$) $V_N = 169$ m/s.

the entrainment rate tends to level off. Fig. 4A also shows the entrainment rates predicted from the model. It can be observed from Fig. 4A that the predicted values of entrainment rate match well with those observed experimentally. It can also be seen from Fig. 4A that the entrainment rate increases with an increase in the liquid level in the tank. The driving force for the liquid entrainment rate can be defined as the pressure difference between the liquid surface at the suction chamber (1 atm) and the pressure at the throat exit. When the nozzle velocity increases, the momentum generated by air jet increases and hence the liquid entrainment in the ejector increases. At low values of the nozzle velocity, the rate of increase of the driving force will be less than the rate of increase of pressure drop. As the nozzle velocity increases to higher values, the driving force tends to level off, and the pressure drop starts increasing rapidly. As a result, the entrainment tends to level off at higher nozzle velocities. Increase in the hydrostatic head, due to increase in the liquid level, provides an additional driving force for the liquid to get entrained. Hence, when the liquid level is increased the entrainment rate also increases.

Fig. 4B shows the effect of nozzle velocity on the pressure profile (obtained from the semi-empirical model) in the ejector as a function of the axial distance. It can be seen clearly that the gas phase undergoes major pressure changes in the nozzle. The pressure drop in the throat and the column are much smaller as compared to the pressure loss in the converging section. The total pressure drop range across the ejector measured experimentally in this work has been 0.04–0.8 atm. The pressure drop across the ejector is significant when compared to the inlet pressures that range from 1.04 to 1.8 atm. The maximum pressure drop takes place in the nozzle that can be seen from the pressure profiles shown later (Fig. 4B). Hence, the compressibility of air in the nozzle becomes significant. The compressibility of air here has already been considered. In the throat and the straight tube of the ejector, the compressibility effects are negligible (especially since their lengths are small). The two-phase flow in these straight tubes has, therefore, been modeled using the new two-phase pressure drop relationship (Eq. (26)). Fig. 4B shows that when the nozzle velocity is increased, the pressure at the throat exit decreases and hence the entrainment rate increases. Thus, the semi-empirical model is able to quantitatively explain the observed behavior.

Fig. 5 shows the effect of area ratio (A_T/A_N) ranging from 4.48 ($D_N = 0.012$ m) to 40.32 ($D_N = 0.004$ m) on the entrainment rate for a fixed nozzle velocity ($V_N = 132$ m/s) and throat diameter ($D_T = 0.0254$ m). The entrainment rate is given both in terms of experimentally measured value and predicted value from the model. On increasing the nozzle diameter from 0.004 to 0.008 m, the liquid entrainment rate increases and on further increasing the diameter to 0.012 m, the entrainment rate decreases. When the nozzle diameter was increased from 0.004 to 0.008 m, the entrainment rate increased because the larger diameter of the air jet and subsequent larger interfacial area increased the momentum transfer from air to water. However, a further increase in the nozzle diameter causes the area of the air jet to increase, which in turn reduces in the annular area available for water flow. As a result, the pressure drop in the throat increases very rapidly at
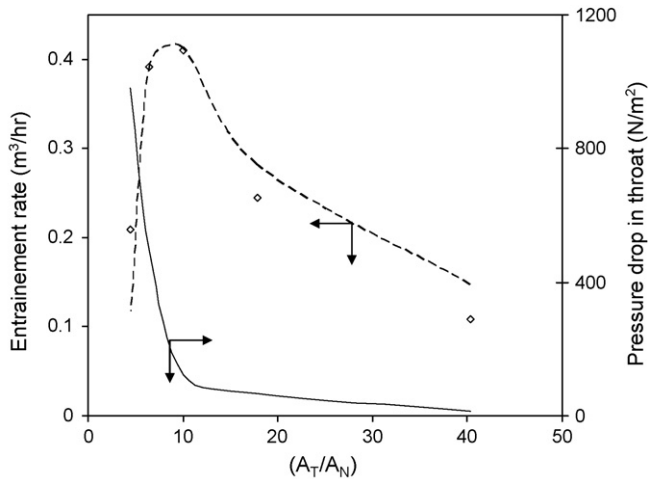
Fig. 5. Effect of area ratio (A_T/A_N) on entrainment rate and throat pressure drop for LH = 0.40 m, H_T = 0.1 m, D_T = 0.0254 m and gas velocity = 129 m/s. (□) Entrainment rate (measured), (—) throat pressure drop, (- - -) entrainment rate (predicted from model).

this point (Fig. 5) that also corresponds to the highest entrainment rate. Kandakure et al. [37] have investigated this aspect in detail with the CFD simulations. It was shown by the authors that at bigger nozzle diameters (i.e. lower value of A_T/A_N), a substantial amount of the entrained fluid re-circulates within the converging section of the ejector. This is primarily due to the reduction in the available area for the flow of the entrained fluid.

Several authors have reported in the past that there is an optimum value of the area ratio, however, no explanations were provided by them. The optimum D_N/D_T ratio in this work corresponds to 0.31 and is in good agreement with the reported values in the literature. Biswas and Mitra [11] have reported optimum D_N/D_T ratio to be in the range of 0.223–0.258. Rylek and Zahradnik [19] have reported the optimum D_N/D_T ratio to be 0.33. Bando et al. [21] have reported the optimum nozzle diameter to be 0.010–0.030 m and D_N/D_T ratio to be 0.l6–0.5, for a H_T/D_T ratio of 20. Zahardnik et al. [2] have reported that as the nozzle diameter approaches the throat diameter, the entrainment rate decreases because the throat gets entirely filled with the motive fluid.

4.3. Effect of nozzle velocity, liquid level and area ratio on fractional liquid hold-up

From the liquid hold-up values measured experimentally, an empirical correlation has been developed in this work to predict the liquid hold-up. The liquid hold-up is related to P/V and area ratio (A_T/A_N) with R^2 of 0.91 as given below:

$$\varepsilon_L = 0.3\left(\frac{P}{V}\right)^{-0.2}\left(\frac{A_T}{A_N}\right)^{0.2} \tag{28}$$

Fig. 6 shows the parity plot obtained between experimental and the predicted liquid hold-up values that include all the data with variation in nozzle velocity, nozzle diameter and liquid level.
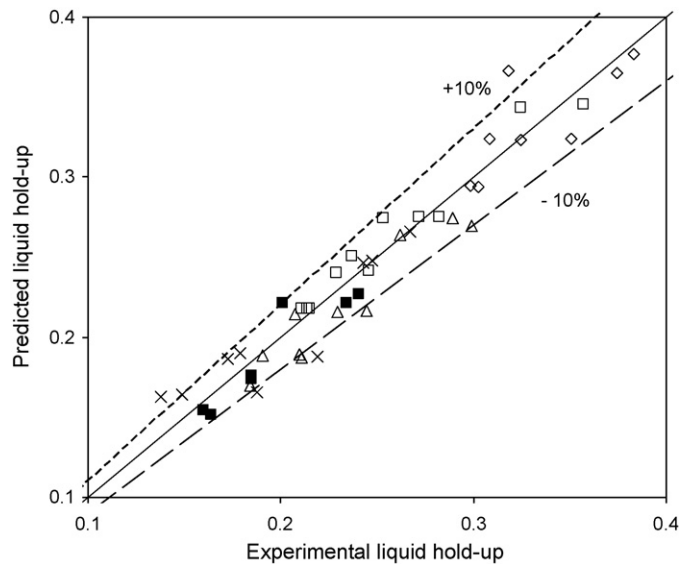

Fig. 6. Parity plot between experimental and predicted liquid hold-up. (◇) A_T/A_N = 40.32, (□) A_T/A_N = 17.92, (△) A_T/A_N = 10.08, (■) A_T/A_N = 6.45, (×) A_T/A_N = 4.48.

Fig. 7 shows the effect of nozzle velocity on liquid hold-up in the ejector. Fig. 7 shows both the experimental and predicted values of liquid hold-up plotted against nozzle velocity. For a particular nozzle diameter, when the nozzle velocity is increased, the air mass flow rate increases. The increase in mass flow rate should increase the liquid entrainment rate. However, the increase in the air mass flow rate is higher than the increase in the liquid entrainment rate (refer Fig. 4A). Hence, the liquid hold-up in the ejector decreases with increase in nozzle velocity.

Fig. 7 also shows the effect of liquid level on the liquid hold-up. For a constant nozzle velocity, when the liquid level is
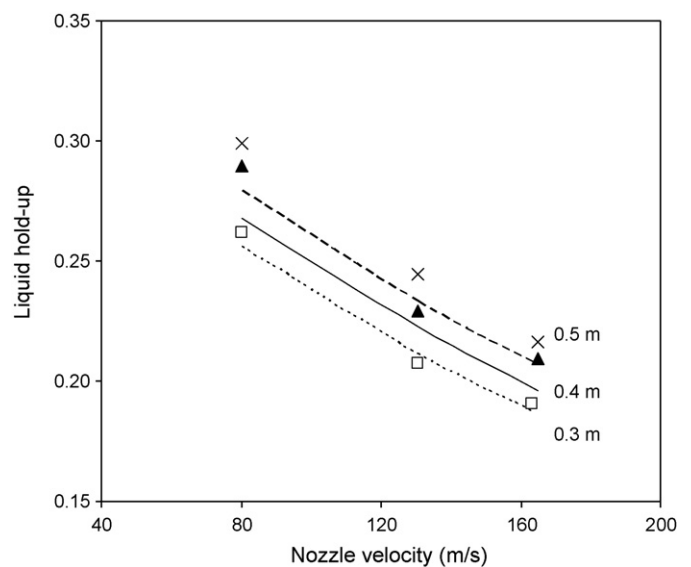

Fig. 7. Effect of nozzle velocity and liquid level on liquid hold-up for H_T = 0.1 m, D_T = 0.0254 m and D_N = 0.008 m. The points indicate experimental values while the lines indicate the predicted values. (□) LH = 0.3 m, (▲) LH = 0.4 m, (×) LH = 0.5 m, (· · ·) LH = 0.3 m, (—) LH = 0.4 m, (- - -) LH = 0.5 m.
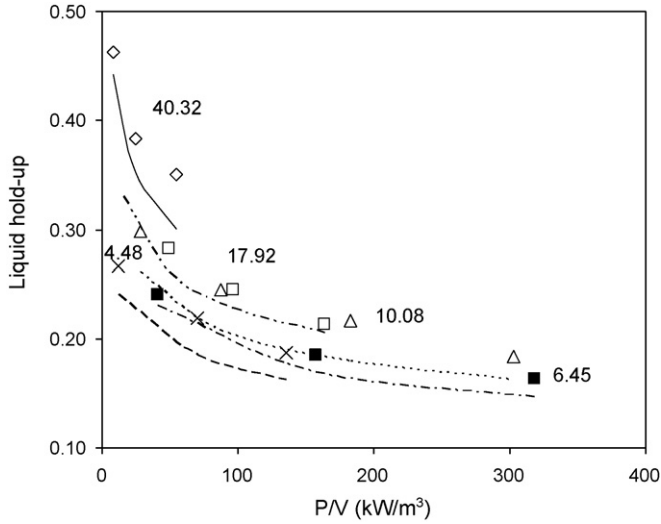
Fig. 8. Effect of area ratio on liquid hold-up for $D_T = 0.0254$ m, $H_T = 0.1$ m and LH = 0.5 m. The points indicate experimental values while the lines indicate the predicted values. ($\Diamond$) $A_T/A_N = 40.32$, ($\Box$) $A_T/A_N = 17.92$, ($\triangle$) $A_T/A_N = 10.08$, ($\blacksquare$) $A_T/A_N = 6.45$, ($\times$) $A_T/A_N = 4.48$, (—) $A_T/A_N = 40.32$, (–··–) $A_T/A_N = 17.92$, (–––) $A_T/A_N = 10.08$, (–·–) $A_T/A_N = 6.45$, (- - -) $A_T/A_N = 4.48$.

increased, the liquid entrainment rate into the ejector increases (refer Fig. 4A; due to increase in additional driving force provided by the increase in liquid level). Hence, the liquid hold-up increases with the increase in the liquid level at the same nozzle velocity.

Fig. 8 shows the effect of power per unit volume of the ejector (P/V) on liquid hold-up for different area ratios (ranging from 4.48 ($D_N = 0.012$ m) to 40.32 ($D_N = 0.004$ m)) for a throat diameter $D_T = 0.0254$ m and LH = 0.5 m. Fig. 8 shows that for a constant P/V, when the nozzle diameter is increased, the liquid hold-up decreases. This is because, for a constant P/V, when the nozzle diameter is increased, the air flow rate and liquid entrainment rate increase. However, the increase in air flow rate is much higher than the increase in the liquid entrainment rate (as explained in the earlier section) and hence the liquid hold-up decreases.

The correlation developed here, Eq. (28), indicates that when the P/V increases, the liquid hold-up decreases. The increase in amount of air is higher than increase in entrainment rate on increasing the P/V and hence the liquid hold-up is decreases with an increase in P/V. When the area ratio is increased, the entrained liquid flow rate decreases and hence liquid hold-up decreases.

4.4. Effect of nozzle velocity, liquid level and area ratio on interfacial area

From the interfacial values obtained from experimentation, an empirical correlation has been developed in this work to predict the interfacial values. In this work, the interfacial area has been correlated with (P/V), liquid hold-up and the area ratio with R^2 of 0.90 as shown below:

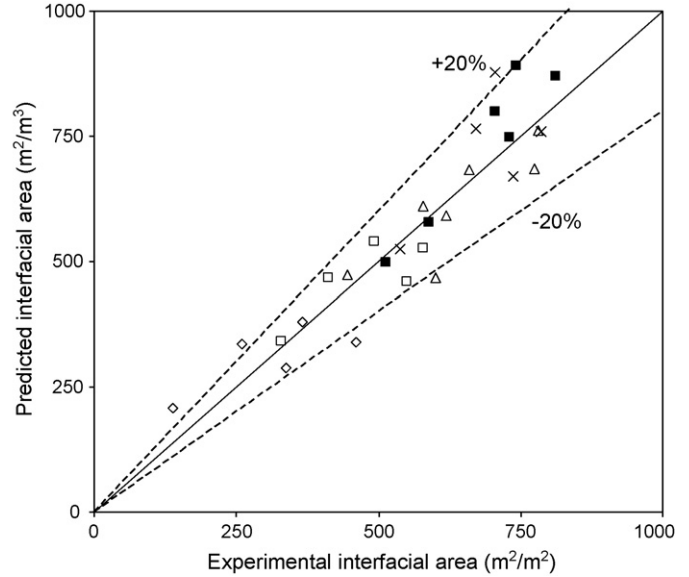$$a = 1530 \left(\frac{P}{V}\right)^{0.4} \varepsilon_L \left(\frac{A_T}{A_N}\right)^{-0.5} \quad (29)$$

Fig. 9. Parity plot between experimental and predicted interfacial area (a). ($\Diamond$) $A_T/A_N = 40.32$, ($\Box$) $A_T/A_N = 17.92$, ($\triangle$) $A_T/A_N = 10.08$, ($\blacksquare$) $A_T/A_N = 6.45$, ($\times$) $A_T/A_N = 4.48$.

Fig. 9 shows the parity plot obtained between experimental and the predicted interfacial area that includes all the data with variation in nozzle velocity, nozzle diameter and liquid level.

Fig. 10 shows the effect of nozzle velocity on interfacial area for $D_N = 0.008$ m. On increasing the nozzle velocity, the interfacial area increases. This can be explained from the droplet diameter generated in the ejector. The droplet diameter was estimated using the liquid hold-up values measured experimentally using equation given below
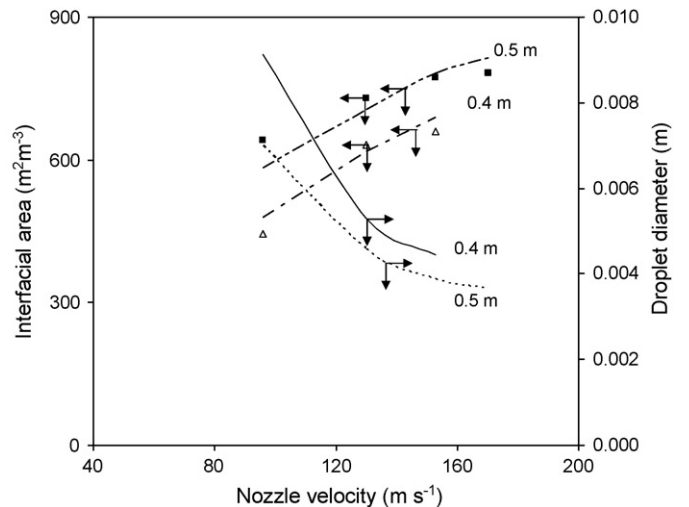
$$D_P = \frac{6\varepsilon_L}{a} \quad (30)$$

Fig. 10. Effect of nozzle velocity and liquid level on the interfacial area for $D_N = 0.008$ m, $D_T = 0.0254$ m, $H_T = 0.1$ m. Interfacial area: ($\triangle$) LH = 0.4 m (experimental), ($\blacksquare$) LH = 0.5 m (experimental), (–··–) LH = 0.4 m (predicted), (–·–) LH = 0.5 m (predicted). Droplet diameter: (—) LH = 0.4 m (estimated), (- - -) LH = 0.5 m (estimated).
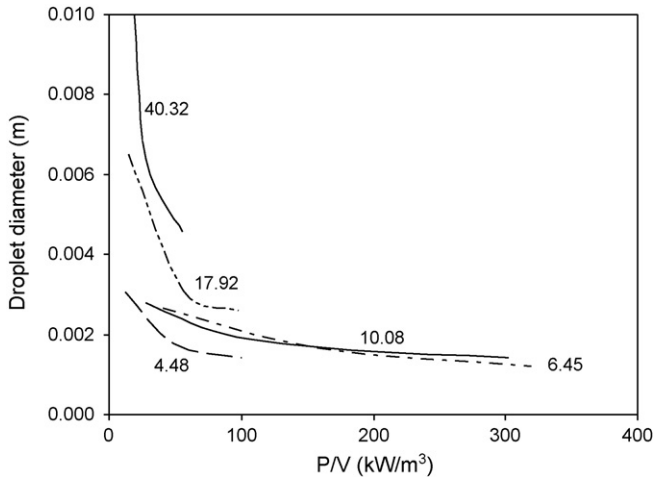
Fig. 11. Effect of area ratio and power per unit volume (P/V) on droplet diameter for $D_T = 0.0254$ m, $H_T = 0.1$ m and LH = 0.5 m. (—) $A_T/A_N = 40.32$, (– · · –) $A_T/A_N = 17.92$, (· · ·) $A_T/A_N = 10.08$, (– · –) $A_T/A_N = 6.45$, (- - -) $A_T/A_N = 4.48$.

Fig. 12. Effect of area ratio and power per unit volume (P/V) on interfacial area for $D_T = 0.0254$ m, $H_T = 0.1$ m and LH = 0.5 m. The points indicate experimental values while the lines indicate the predicted values. (◇) $A_T/A_N = 40.32$, (□) $A_T/A_N = 17.92$, (△) $A_T/A_N = 10.08$, (■) $A_T/A_N = 6.45$, (×) $A_T/A_N = 4.48$, (—) $A_T/A_N = 40.32$, (– · · –) $A_T/A_N = 17.92$, (· · ·) $A_T/A_N = 10.08$, (– · –) $A_T/A_N = 6.45$, (- - -) $A_T/A_N = 4.48$.

Fig. 10 also shows the effect of nozzle velocity on the size of droplet diameter formed. From Fig. 10, it can be seen that an increase in the nozzle velocity causes a reduction in the droplet diameter. Increase in nozzle velocity increases the specific power input to the system. This increases the shear action that eventually decreases the size of the droplet. This leads to an increase in the interfacial area. Fig. 10 also shows the effect of liquid level on interfacial area. It shows that an increase in liquid level the interfacial area increases. Fig. 7 shows that on increasing the liquid level from 0.4 to 0.5 m, the liquid hold-up increases, as a result the interfacial area increases.

Fig. 11 shows the effect of P/V on droplet diameter for different area ratio (4.48–40.32). When the P/V is increased, the droplet diameter decreases. When the P/V is increased, the amount of energy dissipation increases which subsequently increases the dispersion leading to formation of finer droplets. Hence, the droplet diameter decreases with increase in P/V. For a constant P/V, when the nozzle diameter is increased, the size of the air jet increases. This decreases the annular area occupied by water in the throat region. This increases the shear between these two phases, which leads to the higher energy dissipation rate. Because of higher energy dissipation rates, the droplets formed are smaller on increasing the nozzle diameter.

Fig. 12 shows the effect of P/V on interfacial area for different area ratio (A_T/A_N) (ranging from 4.48 ($D_N = 0.012$ m) to 40.32 ($D_N = 0.004$ m)) for a constant $D_T = 0.0254$ m and LH = 0.5 m with help of both experimental and predicted values. For all area ratio values, when P/V is increased the interfacial area also increases. For a constant P/V, when the nozzle diameter is increased, the interfacial area increases. This is because of decrease in droplet diameter on increasing the P/V and nozzle diameter (refer Fig. 11).

From the correlation developed, it can be seen that the interfacial area increases with increase in P/V due to the formation of smaller droplets at higher P/V. Interfacial area increases at a given liquid hold-up due to the increased shear between air and water. Interfacial area increases with nozzle diameter due to an
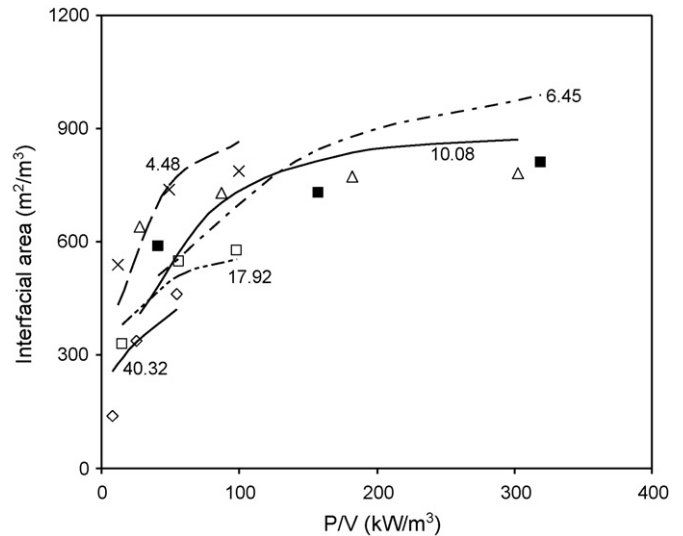
increase in energy dissipation rate arising out of an increase in the area of the air jet in the throat.

4.5. Effect of nozzle velocity, liquid level and area ratio on $k_L a$

From the experimental values of $k_L a$, an empirical correlation has been developed with R^2 of 0.95 as given below:

$$k_L a = 1.7 \left(\frac{P}{V} \right)^{0.4} \varepsilon_L^{0.5} \left(\frac{A_T}{A_N} \right)^{-0.45} \tag{31}$$

Fig. 13 shows the parity plot obtained between experimental and the predicted $k_L a$ that includes all the data with variation in nozzle velocity, nozzle diameters and liquid levels.

Fig. 14 shows the effect of nozzle velocity and liquid level on $k_L a$. When the nozzle velocity increases, both the liquid entrainment rate (Fig. 4A) and interfacial area (Fig. 10) increases. Because of this combined effect, $k_L a$ also increases with increase in gas velocity. Fig. 14 also shows that $k_L a$ increases with increase in liquid level in the tank. Because, for a certain nozzle velocity when the liquid level is increased the fractional liquid hold-up also increases due to increase in the entrainment rate (Fig. 7).

Fig. 15 shows the effect of area ratio (A_T/A_N) (ranging from 4.48 ($D_N = 0.012$ m) to 40.32 ($D_N = 0.004$ m)) on $k_L a$ for a throat diameter ($D_T = 0.0254$ m). For a constant P/V, when the nozzle diameter is increased, the $k_L a$ increases.

4.6. Comparison with other gas–liquid contactors

The values of mass transfer parameters observed in ejectors are high and it is essential to compare these values with that of other conventional gas–liquid contactors. In this work, the per-
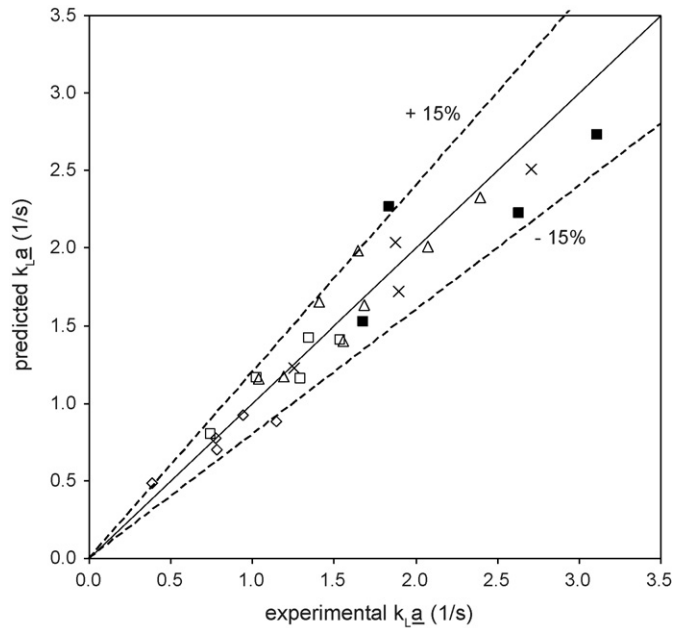
Fig. 13. Parity plot between experimental and predicted $k_L a$. ($\Diamond$) $A_T/A_N = 40.32$, ($\Box$) $A_T/A_N = 17.92$, ($\triangle$) $A_T/A_N = 10.08$, ($\blacksquare$) $A_T/A_N = 6.45$, ($\times$) $A_T/A_N = 4.48$.

formance of ejectors are compared with that of bubble column and stirred tank in terms of $k_L a$ and oxygen transfer efficiency (the amount of oxygen transferred per kW-h, OTE). Correlations available in the literature [38,39] were used to estimate the values of $k_L a$ and OTE of stirred tank and bubble column, respectively.

4.6.1. Comparison in terms of $k_L a$

In this section, the procedure used to estimate the values of $k_L a$ in stirred tank and bubble column has been discussed in detail. Stirred tank with tank height to tank diameter (D_s) ratio of unity and tank diameter to impeller diameter (D_I) ratio of
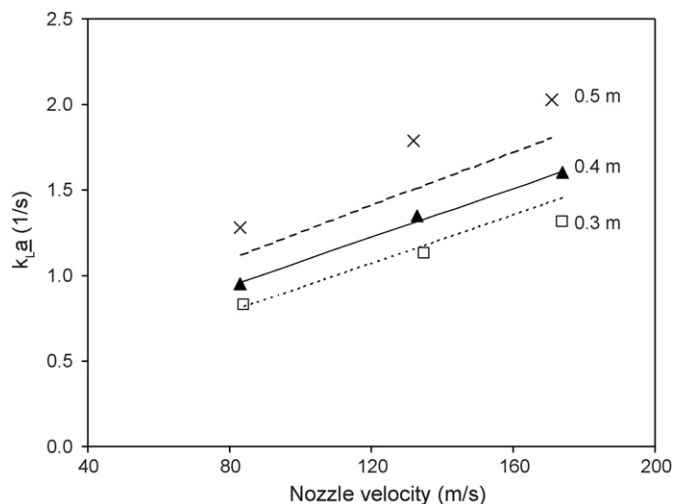

Fig. 14. Effect of nozzle velocity and liquid level on $k_L a$ for $D_N = 0.008$ m, $D_T = 0.0254$ m, $H_T = 0.1$ m. The points indicate experimental values while the lines indicate the predicted values. ($\Box$) LH = 0.3 m, ($\blacktriangle$) LH = 0.4 m, ($\times$) LH = 0.5 m, (- - -) LH = 0.3 m, (——) LH = 0.4 m, ($\cdots$) LH = 0.5 m.
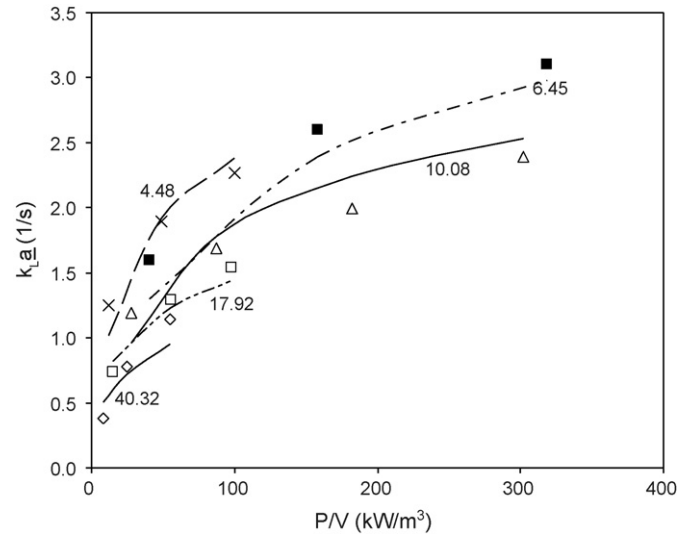

Fig. 15. Effect of area ratio and power per unit volume (P/V) on the $k_L a$ for $D_N = 0.008$ m, $D_T = 0.0254$ m, HT = 0.1 m and LH = 0.5 m. The points indicate experimental values while the lines indicate the predicted values. ($\Diamond$) $A_T/A_N = 40.32$, ($\Box$) $A_T/A_N = 17.92$, ($\triangle$) $A_T/A_N = 10.08$, ($\blacksquare$) $A_T/A_N = 6.45$, ($\times$) $A_T/A_N = 4.48$, ($\_\_$) $A_T/A_N = 40.32$, ($-\cdot\cdot-$) $A_T/A_N = 17.92$, ($\cdots$) $A_T/A_N = 10.08$, ($-\cdot-$) $A_T/A_N = 6.45$, (- - -) $A_T/A_N = 4.48$.

3 was considered. The gas hold-up in the stirred tank can be estimated using following correlation:

$$\varepsilon_G = 3.54 \left(\frac{D_I}{D_s} \right)^{2.08} Fr^{0.51} Fl^{0.43} \tag{32}$$

For example, if the impeller speed, power number and velocity of air sparged into the tank are assumed to be 4 rps (240 rpm), 5 and 0.01 m/s, respectively, the hold-up estimated from Eq. (32) is 0.067 (i.e. 6.7%). The correlation to estimate bubble diameter and interfacial area are given below:

$$D_B = 2 \left(\frac{(P_G / V_L)^{0.4} \rho_L^{0.2}}{\sigma^{0.6}} \right)^{-1} \varepsilon_G^{0.5} + 0.0009 \tag{33}$$

$$a = 6 \frac{\varepsilon_G}{D_B} \tag{34}$$

For the above-mentioned case, the bubble diameter and interfacial area estimated were 0.004 m and 97 m^2/m^3. Assuming typical value for k_L to be 2×10^4 m/s, the $k_L a$ value was found to be 0.019 s^{-1}. Similarly, the value of $k_L a$ was estimated as a function of P/V by varying the impeller speed from 4 to 15 rps.

Bubble column with height to diameter ratio of 5 was used for comparison. Assuming that the liquid is batch wise, gas-hold-up can be estimated using the following equation:

$$\frac{V_G}{\varepsilon_G} = C_0 V_G + C_1 \tag{35}$$

In this relation, C_0 indicates the extent of non-uniformity in hold up profile and C_1 indicates the slip velocity. Typically, values of C_0 range from 1 to 2 while C_1 range from 0.20 to 0.35. C_0 and C_1 depend upon physicochemical properties of the system, height to diameter ratio, sparger design, etc. For example, if $C_0 = 2$ and $C_1 = 0.35$, the gas hold-up would be $\varepsilon_G = 0.11$ for

gas velocity of 0.05 m/s, $\varepsilon_G = 0.267$ for gas velocity of 0.2 m/s and $\varepsilon_G = 0.316$ for gas velocity of 0.3 m/s.

The gas–liquid mass transfer coefficient is estimated using the correlation given below which has been found to be valid for a wide range of bubble column operation:

$$\left(\frac{k_L a D_B^2}{D_L}\right) = 0.62 \left(\frac{\mu_L}{\rho_L D_L}\right)^{0.5} \left(\frac{g \rho_L D_B^2}{\sigma}\right)^{0.33} \left(\frac{g \rho_L^2 D_B^3}{\mu_L^2}\right)^{0.29}$$
$$\times \left(\frac{V_G}{\sqrt{g D_B}}\right)^{0.68} \left(\frac{\rho_G}{\rho_L}\right)^{0.04} \quad (36)$$

In the above correlation, the bubble diameter (D_B) is assumed to be 0.004 m a typical value for an air-water system. The corresponding physical properties of air and water were used in the correlation. For a gas velocity (V_G) of 0.05 m/s, the $k_L a$ estimated from Eq. (36) was found to be 0.022 s^{-1}. The above relation shows that $k_L a \propto V_G^{0.68}$, since $P/M \propto V_G$, $k_L a \propto (P/M)^{0.68}$. Hence, the $k_L a$ can be related to D_B as $k_L a \propto D_B^{-0.81}$. Similarly, the values of $k_L a$ were estimated as a function of P/V by varying the V_G from 0.05 to 0.7 m/s.

Fig. 16A shows the comparison of $k_L a$ values of ejector with that of stirred tank reactor [38] and bubble column [39] as a function of power per unit volume of the contactor. It shows that the $k_L a$ values produced in ejectors are very high compared to other conventional gas–liquid contactors. Higher P/V values in the ejector are due to the higher pressure drop across the ejector. This higher power dissipation decreases the droplet size and hence the interfacial area increases. This leads to higher values of $k_L a$ in ejector system.

4.6.2. Comparison in terms of OTE

Another way of comparison of mass transfer performance is to compute the values of oxygen transfer efficiency. In order to do this, it is first necessary to estimate the rate of mass transfer:

$$R_A a = k_L a \{[O_2^*] - [O_2]_0\} \quad (37)$$

The maximum rate of oxygen transfer was estimated by assuming the bulk (dissolved) oxygen concentration to zero ($[O_2]_0 = 0$) and taking the typical value of $[O_2^*]$ for oxygen solubility in water as 8 mg/l (0.008 kg/m^3). The total rate of oxygen transfer was estimated using the following relation:

$$(R_A a)_{Total} = k_L a [O_2^*] V \quad (38)$$

The OTE was estimated from the following expression:

$$OTE = 3600 k_L a [O_2^*] \frac{V}{P} \quad (39)$$

Fig. 16B shows the comparison of OTE values of ejector with that of bubble column and stirred tank as a function of (P/V). Fig. 16B shows that as (P/V) increases, the OTE decreases for all the contactors. It has been observed that $k_L a$ increases with an increase in (P/V), however, increase in (P/V) is higher when compared to the increase in the values of $k_L a$. Hence, the decrease in OTE is observed with an increase in (P/V). Fig. 16B also shows that for a given (P/V), the stirred tank has the lowest
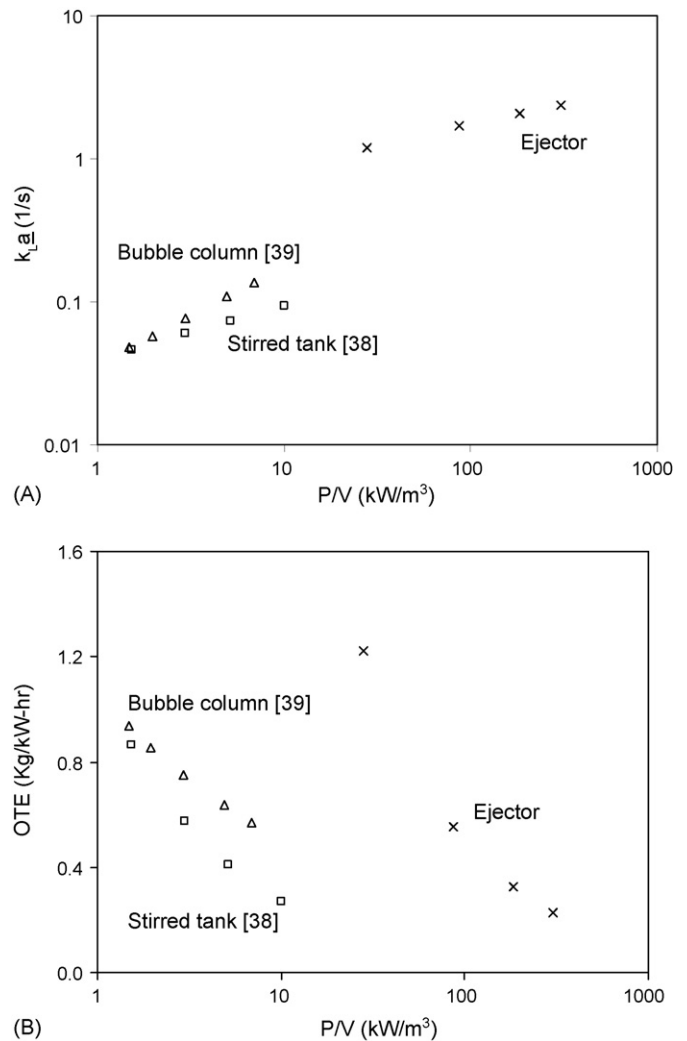

Fig. 16. (A) Comparison of $k_L a$ values of ejector with other gas–liquid contactors as a function of (P/V), (□) stirred tank [39], (△) bubble column [39], (×) ejector D_N = 8 mm. (B) Comparison OTE of ejector with other gas–liquid contactors as a function of (P/V). Legend same as (A).

OTE and the highest value of OTE is observed with ejector. This difference is due the different flow pattern and dispersion observed in these contactors. This confirms ejector as a better gas–liquid contactors in terms of mass transfer characteristics.

5. Process implications

In the process, the throughput of the product is normally not changed. Therefore, it is essential to analyze the effect of ejector configuration on the hydrodynamics and the performance of the ejectors at different mass flow rates. The results show that the ratio of the throat diameter to the nozzle diameter plays a crucial role in determining the hydrodynamics and the performance of the ejectors. Fig. 17A shows the effect of air mass flow rate on pressure drop for different nozzle diameters. For the same mass flow rate, when the nozzle diameter was increased from 6 to 12 mm there was 25% reduction in the pressure drop. Fig. 17B and C show the effect of air mass flow rate on interfacial area and $k_L a$, respectively, for different area ratios. On increasing the
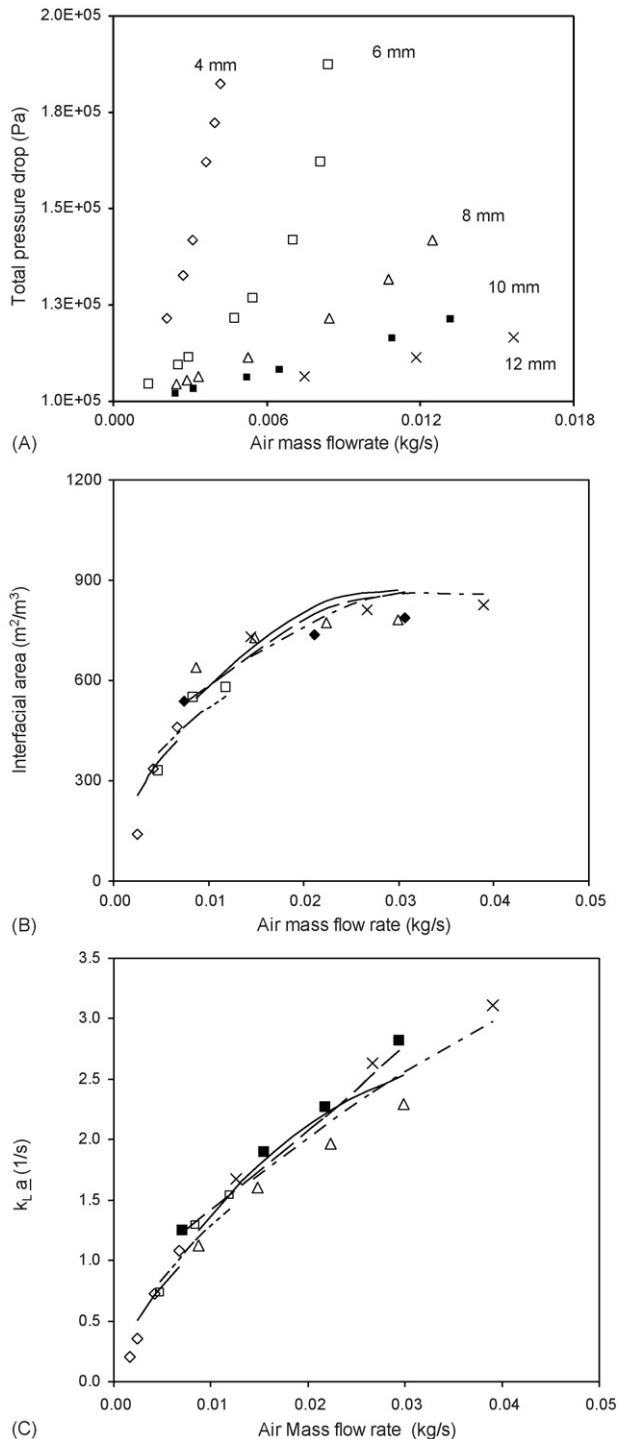
Fig. 17. (A) Effect of nozzle diameter on total pressure drop in the ejector for $D_T = 0.0254$ m, $H_T = 0.01$ m and LH $= 0.5$ m. ($\Diamond$) $A_T/A_N = 40.32$, ($\Box$) $A_T/A_N = 17.92$, ($\triangle$) $A_T/A_N = 10.08$, ($\blacksquare$) $A_T/A_N = 6.45$, ($\times$) $A_T/A_N = 4.48$. (B). Effect of air mass flow rate on interfacial area for LH $= 0.5$ m, $H_T = 0.1$ m and $D_T = 0.0254$ m. The points indicate experimental values while the lines indicate the predicted values. ($\Diamond$) $A_T/A_N = 40.32$, ($\Box$) $A_T/A_N = 17.92$, ($\triangle$) $A_T/A_N = 10.08$, ($\blacksquare$) $A_T/A_N = 6.45$, ($\times$) $A_T/A_N = 4.48$, (—) $A_T/A_N = 40.32$, (– ·· –) $A_T/A_N = 17.92$, (···) $A_T/A_N = 10.08$, (– · –) $A_T/A_N = 6.45$, (- - -) $A_T/A_N = 4.48$. (C) Effect of air mass flow rate on $k_L a$ for LH $= 0.5$ m, $H_T = 0.1$ m and $D_T = 0.0254$ m. The points indicate experimental values while the lines indicate the predicted values. ($\Diamond$) $A_T/A_N = 40.32$, ($\Box$) $A_T/A_N = 17.92$, ($\triangle$) $A_T/A_N = 10.08$, ($\blacksquare$) $A_T/A_N = 6.45$, ($\times$) $A_T/A_N = 4.48$, (—) $A_T/A_N = 40.32$, (– ·· –) $A_T/A_N = 17.92$, (···) $A_T/A_N = 10.08$, (– · –) $A_T/A_N = 6.45$, (- - -) $A_T/A_N = 4.48$.

mass flow rate, both $k_L a$ and interfacial area increase. However, for a constant mass flow rate the area ratio has little effect on $k_L a$ and interfacial area. At a given mass flow rate, when the nozzle diameter is increased, the nozzle velocity goes down. Therefore, the driving force goes down but at lower area ratios, the entrainment rate increases (Fig. 5). Because of this combined effect, the increase in nozzle diameter for a constant mass flow rate has not affected the mass transfer characteristics. Combination of Fig. 17A–C show that for a given mass flow rate of air the operating cost can be reduced (lower pressure drop) with the same extent of gas–liquid contacting (with same level of mass transfer characteristics) by using an optimized value of the nozzle diameter.

6. Conclusions

In the present work, hydrodynamic characteristics of ejectors using air as the motive fluid and water as the entrained fluid have been investigated. Experiments have been performed over a wide range of ejector configurations ($D_N = 0.004$–0.012 m, $D_T = 0.02$–0.04 m, $H_T = 0.05$ and 0.1 m, nozzle velocity $= 27$–210 m/s and liquid level $= 0.25$–0.50 m). It was observed that the liquid entrainment rate increases with an increase in the liquid level and the nozzle velocity. The entrainment rate was found to be highest corresponding to area ratio of about 10. This is because, the pressure drop was found to increase rapidly with a reduction in area ratio below 10. A semi-empirical model has been developed to predict the performance of the ejector. The model predictions have been found to be in good agreement with the experimental measurements. The effects of ejector geometry and operating conditions on the liquid entrainment have been explained on the basis of the model developed in terms of the pressure drop and the driving force. The mass transfer coefficient and interfacial area increases with increase in nozzle velocity and P/V. Correlations were developed to predict the mass transfer coefficient and interfacial area and the predictions match with experimental within $\pm 20\%$ error. Hence, by optimizing the nozzle diameter, the reduction in operating cost (reduction in pressure drop of about 25%) can be achieved without significantly affecting the mass transfer characteristics of the ejectors. The performance of ejector systems has been compared with the conventional contactors like stirred tanks and bubble columns.

References

[1] P.H.M.R. Cramers, A.A.C.M. Beenackers, Influence of the ejector configuration, scale and the gas density on the mass transfer characteristics of gas–liquid ejectors, Chem. Eng. J. 82 (2001) 131–141.
[2] J. Zahradnik, M. Fialova, V. Linek, J. Sinkule, J. Renickoca, F. Kastanek, Dispersion efficiency of ejector-type gas distributors in different operating modes, Chem. Eng. Sci. 52 (24) (1997) 4499–4510.

[3] P. Havelka, V. Linek, J. Sinkule, J. Zahradnik, M. Fialova, Hydrodynamics and mass transfer characteristics of ejector loop reactors, Chem. Eng. Sci. 55 (2000) 535–549.

[4] D.K. Acharjee, P.A. Bhat, A.K. Mitra, A.N. Roy, Studies on momentum transfer in vertical liquid jet ejectors, Indian J. Technol. 13 (1975) 205–210.

[5] A. Ben Brahim, M. Prevost, R. Bugarel, Momentum transfer in a vertical down flow liquid jet ejector: case of self gas aspiration and emulsion flow, Int. J. Multiphase Flow 10 (1) (1984) 79–94.

[6] S.M. Dave, H.M. Sadhukhan, O.A. Novaro, Heavy Water, Quest publications, Mumbai, India, 1997.

[7] G.S. Davies, A.K. Mitra, A.N. Roy, Momentum transfer studies in ejectors, Ind. Eng. Chem. Process Des. Dev. 6 (3) (1967) 293–299.

[8] P.A. Bhat, A.K. Mitra, A.N. Roy, Momentum transfer in a horizontal liquid jet ejector, Can. J. Chem. Eng. 50 (1975) 313–317.

[9] N.N. Dutta, K.V. Raghavan, Mass transfer and hydrodynamic characteristics of loop reactors with down flow liquid jet ejectors, Chem. Eng. J. 36 (1987) 111–121.

[10] S.R. Bhutada, V.G. Pangarkar, Gas induction and hold-up characteristics of liquid jet loop reactors, Chem. Eng. Commun. 61 (1987) 239–261.

[11] M.N. Biswas, A.K. Mitra, Momentum transfer in horizontal multi-jet liquid–gas ejector, Can. J. Chem. Eng. 59 (1981) 634–637.

[12] H. Henzler, Design of ejectors for single phase material systems, Germ. Chem. Eng. 6 (1983) 292–300.

[13] R.G. Cunningham, Gas compression with the liquid jet pump, Trans. ASME—J. Fluids Eng. 96 (1974) (1974) 203–215.

[14] M. Mandal, G. Kundu, D. Mukherjee, Energy analysis and air entrainment in an ejector induced down flow bubble column with Non-Newtonian motive fluid, Chem. Eng. Technol. 28 (2) (2005) 210–218.

[15] T. Otake, S. Tone, R. Kuboi, Y. Takahashi, K. Nakao, Dispersion of a gas by a liquid jet ejector, Int. Chem. Eng. 21 (1981) 72–80.

[16] J. Zahradnik, J. Kratochvil, F. Kastanek, M. Rylek, Energy effectiveness of bubble column reactors with sieve tray and ejector type gas distributors, Chem. Eng. Commun. 15 (1982) 27–40.

[17] J. Zahradnik, J. Kratochvil, F. Kastanek, M. Rylek, Hydrodynamic characteristics of gas–liquid beds in contactors with ejector type gas distributors, Collect. Czech. Chem. Commun. 47 (1982) 1939–1949.

[18] S. Ogawa, H. Yamaguchi, S. Tone, T. Otake, Gas–liquid mass transfer in the jet reactor with liquid jet ejector, J. Chem. Eng. Jpn. 16 (1983) 419–425.

[19] M. Rylek, J. Zahradnik, Design of Venturi-tube gas distributors for bubble type reactors, Collect. Czech. Chem. Commun. 49 (1984) 1939–1948.

[20] J. Zahradnik, J. Kratochvil, M. Rylek, Gas holdup and interfacial mass transfer in gas–liquid tower contactors with ejector type gas distributors, Collect. Czech. Chem. Commun. 50 (1985) 2535–2544.

[21] Y. Bando, M. Kuraishi, M. Nishimura, I. Takeshita, The characteristics of a bubble column with a gas-suction type, simultaneous gas–Liquid injection-nozzle, Int. Chem. Eng. 30 (1990) 729–737.

[22] C.A.M.C. Dirix, K. van der Wiele, Mass transfer in jet loop reactors, Chem. Eng. Sci. 45 (1990) 2333–2340.

[23] P.H.M.R. Cramers, L.L. van Dierendonck, A.A.C.M. Beenackers, Influence of the gas density on the gas entrainment rate and gas hold-up in loop venturi reactors, Chem. Eng. Sci. 47 (1992) 2251–2256.

[24] P.H.M.R. Cramers, L.L. van Dierendonck, A.A.C.M. Beenackers, Hydrodynamics and mass transfer characteristics of a loop venturi reactor with a downflow liquid jet ejector, Chem. Eng. Sci. 47 (1992) 3557–3564.

[25] P. Havelka, V. Linek, J. Sinkule, J. Zahradnik, M. Fialova, Effect of the ejector configuration on the gas suction rate and gas hold-up in ejector loop reactors, Chem. Eng. Sci. 52 (1997) 1701–1713.

[26] A. Mandal, G. Kundu, D. Mukherjee, Gas holdup and entrainment characteristics in a modified downflow bubble column with Newtonian and non-Newtonian liquid, Chem. Eng. Process. 42 (2003) 777–787.

[27] A. Mandal, G. Kundu, D. Mukherjee, Interfacial area and liquid-side volumetric mass transfer coefficient in a downflow bubble column, Can. J. Chem. Eng. 81 (2003) 212–219.

[28] M. Moresi, G.B. Gianturco, E. Sebastiani, The ejector-loop fermenter: description and performance of the apparatus, Biotechnol. Bioeng. 25 (12) (1983) 2889–2904.

[29] U. Parasu Veera, J.B. Joshi, Measurement of gas hold-up profiles by Gamma Ray Tomography: effect of sparger design and height of dispersion in bubble columns, Trans. Inst. Chem. Eng. 77A (1999) 303–315.

[30] A.R. Thatte, R.S. Ghadge, A.W. Patwardhan, J.B. Joshi, G. Singh, Local hold-up measurements in sparged and aerated tanks by γ-ray attenuation technique, Ind. Eng. Chem. Res. (2004) 5389–5399.

[31] L.K. Doraiswamy, M.M. Sharma, Heterogeneous Reactions: Analysis, Examples and Reactor Design, vol. 2, Wiley Interscience, New York, 1983.

[32] P.V. Danckwerts, Gas–Liquid Reactions, McGraw Hill, New York, 1970.

[33] P.V. Danckwerts, M.M. Sharma, Chemical methods for measuring interfacial areas and mass transfer coefficients in two-fluid systems, Br. Chem. Eng. 15 (1970) 522–528.

[34] C.E. Lapple, Isothermal and adiabatic flow of compressible fluids, Trans. AIChEngers. 39 (1943) 385.

[35] O. Levenspiel, The discharge of gases from a reservoir through a pipe, AIChE J. 23 (8) (1977) 403–404.

[36] W.J. Davis, The effect of the Froude number in estimating vertical two-phase gas–liquid friction factor, Br. Chem. Eng. 8 (7) (1963) 462–465.

[37] M.T. Kandakure, V.G. Gaikar, A.W. Patwardhan, Hydrodynamic aspects of ejectors, Chem. Eng. Sci. 60 (2005) 6391–6402.

[38] G.B. Tatterson, Fluid Mixing and Gas Dispersion in Agitated Vessels, McGraw Hill, New York, 1991.

[39] W.D. Deckwer, Bubble Column Reactors, Wiley, New York, 1992.